

Distribution and stratigraphy of deposits produced by diluted pyroclastic density currents of the 1982 eruption of El Chichón volcano, Chiapas, Mexico

Teresa Scolamacchia*, and José Luis Macías

*Instituto de Geofísica, Universidad Nacional Autónoma de México,
Ciudad Universitaria, Coyoacán 04510, México D.F., México.*

** teresasc@tonatiuh.igeofcu.unam.mx*

ABSTRACT

The March 29 to April 4, 1982 eruption of El Chichón volcano in southeastern Mexico was characterized by a complex interplay between magmatic and phreatomagmatic eruptive events, that were responsible for the generation of plinian columns and concentrated and diluted density currents. Revision of the stratigraphy indicates that the interaction between magma and hydrothermal acid water played an important role during the last phases of the eruption. Diluted density currents were widely dispersed, mainly to the eastern side of the volcano due to the particular topographic conditions in this area. The overall distribution of pyroclastic surge deposits reflects the dispersal of fallout deposits determined by the direction of tropospheric (ENE) winds at the time of the eruption. This observation suggests that near-ground winds were strong and blowing in the same direction as high altitude (<18 km) winds, thus enhancing the dispersion of the vanishing portions of the pyroclastic density currents.

Key words: pyroclastic density currents, 1982 eruption, El Chichón, Chiapas, Mexico.

RESUMEN

La erupción del volcán El Chichón en el sureste de México, ocurrida del 29 de Marzo al 4 de Abril de 1982, se caracterizó por una alternancia compleja entre eventos magmáticos y freatomagmáticos que generaron columnas plinianas, flujos y oleadas piroclásticas. La estratigrafía de los depósitos indica que la interacción entre magma y agua hidrotermal jugó un papel importante durante las últimas fases de la erupción. Las oleadas piroclásticas fueron ampliamente distribuidas hacia el oriente del volcán debido a las condiciones topográficas presentes en esta dirección. La distribución general de los depósitos de oleada piroclástica refleja la distribución de los depósitos de caída, la cual fue determinada por la dirección de los vientos troposféricos (ENE) durante la erupción. Esto sugiere que los vientos cercanos al terreno eran fuertes y soplaban en la misma dirección que los vientos superiores (< 18 km), influenciando la distribución de las porciones más diluidas de las oleadas piroclásticas.

Palabras clave: oleada piroclástica, erupción de 1982, El Chichón, Chiapas, México.

INTRODUCTION

Pyroclastic surges are turbulent, low particle concentration density currents that move under the effect of gravity (Valentine and Fisher, 2000). The term pyroclastic surge encompasses four main categories of flow and deposits: ground surges, ash cloud surges, base surges (Fisher, 1979; Cas and Wright, 1987), and blast surges (Lipmann and Mollineaux, 1981). Base surge deposits are mainly found in tuff rings, tuff cones and maars related to hydromagmatic activity (Fisher and Waters, 1970; Crowe and Fisher, 1973; Heiken, 1971; Wohletz and Sheridan, 1983; Sohn, 1996). Blast surges are derived from a lateral explosion due to the depressurization of a cryptodome (Fisher *et al.*, 1987; Belousov, 1996). Pyroclastic surge deposits associated with the emplacement of pyroclastic flows are stratified or massive deposits characteristically found at the base (ground surge deposits) and atop (ash cloud surge deposits) of pyroclastic flow deposits (Cas and Wright, 1987). Ground surge deposits are originated during the initial collapse of a plinian column (Sparks and Walker, 1973) and ash cloud surges are derived from the elutriation of fine-grained material from the upper part of a pyroclastic flow during its mixing with the atmosphere (Fisher and Schmincke, 1984). Their distribution is thus intimately associated with that of pyroclastic flows although in the latter case it is less controlled by topography (Fisher, 1995) with low probability of preservation because of post-depositional erosion (Cas and Wright, 1987).

Base surge deposits often form during complex eruptions due to the interaction of magma and external water, where closely-timed explosions occur, producing deposits with a radial distribution around the vent and a dispersion of few kilometers (Moore *et al.*, 1966; Lorenz, 1974; White, 1991; Sohn, 1996). Depending on the relative amounts of magma and external water that interact, as well as the differential flow speed between the two media, two different types of deposits (dry and wet) can be distinguished (Sheridan and Wohletz, 1983; Fisher and Schmincke, 1984; Zimanowski *et al.*, 1997). In these cases, densely stratified sequences related to the passage of many successive and independent currents are produced (Schmincke *et al.*, 1973; Cole and Scarpati, 1993; Dellino *et al.*, 2004a). The risk associated with this kind of volcanic eruptions is thus related to the passage of each independent flow (Valentine, 1998).

The March 29–April 4, 1982 eruption of El Chichón volcano in Chiapas, Mexico, has been considered one of the most violent eruptions in historic times (Tilling, 1989) and was responsible for the reduction of the global temperature in 0.5°C (Toon, 1982). Approximately 2.2×10^{13} g of sulfur was emitted (Luhr and Logan, 2002), while the SO₂ contents inside the eruptive clouds were estimated at 5 to 9 megatons (Krueger *et al.*, 1995). The stratigraphy of the deposits was examined shortly after the eruption (Sigurdsson *et al.*, 1984; 1987) and more than ten years later (Macías, 1994; Macías *et al.*, 1997a). On the basis of seismic and satellite

records, Macías *et al.* (1997a) subdivided the eruption into four phases. Fallout deposits A1 and A2 were produced on March 29 (0532 GMT; phase I) and April 3 (0830 GMT; phase II). One fourth of the central andesitic dome was removed during phase I (Sigurdsson *et al.*, 1984). The most violent eruptive episodes occurred on April 4 (at 0135 and 1122 GMT; phases III–IV, respectively) producing pyroclastic flows, surges and fallouts that destroyed nine villages around the volcano and killed more than 2,000 people. Both magmatic (Sigurdsson *et al.*, 1984; Macías *et al.*, 1997a) and hydromagmatic (Sigurdsson *et al.*, 1987; Macías *et al.*, 1997a) processes were invoked to explain the origin of pyroclastic surge units S1, IU, S2, and S3.

Considering the differing interpretations existent on the origin of pyroclastic surges produced during the 1982 eruption (Sigurdsson *et al.*, 1984, 1987; Macías *et al.*, 1997a), this work is aimed at delucidating the eruptive mechanisms, mode of emplacement, and distribution pattern of these deposits.

LOCATION

El Chichón volcano (Figure 1a) is the youngest volcano of the Chiapanecan Volcanic Arc, a 150 km-long Quaternary belt composed of small volume volcanoes (3–4 km³) oriented NW-SE within the State of Chiapas (Capaul, 1987). The 1982 crater is 1 km wide and 160 m deep, its maximum elevation is 1,100 meters above sea level (hereafter m); it lies inside a Somma crater 1.5 x 2 km wide and 1,150 m in maximum elevation (Figures 1b and 2). Two external domes are located to the SE (Duffield *et al.*, 1984) and to the NW (Macías, 1994). The cone is built on folded Cretaceous marine limestones intercalated with gypsum and alternating sequences of Tertiary shales and marls (Canul and Rocha, 1981), oriented NW-SE and transected by faults with a left-lateral strike slip movement (Macías *et al.*, 1997b; García-Palomo *et al.*, 2004). These structural features control the pattern of rivers and determine the topographic irregularities around the cone (Figure 2). Espíndola *et al.* (2000) concluded that El Chichón was very active during the Holocene, as evidenced by 11 eruptions during the last 8,000 years.

STRATIGRAPHY OF THE 1982 PYROCLASTIC SURGE DEPOSITS

In this work, the term *horizon* indicates a bed(s) emplaced during an eruption unit (Fisher and Schmincke, 1984) of pyroclastic surge clearly distinguishable from contiguous horizons because of their color, sometimes delimited by a red oxidized millimeter layer or erosive surfaces, attesting the occurrence of a defined eruptive event. Bed thickness inside horizons is defined following Ingram (1954) (Table 1). The term *flow unit* refers to a deposit recording the em-

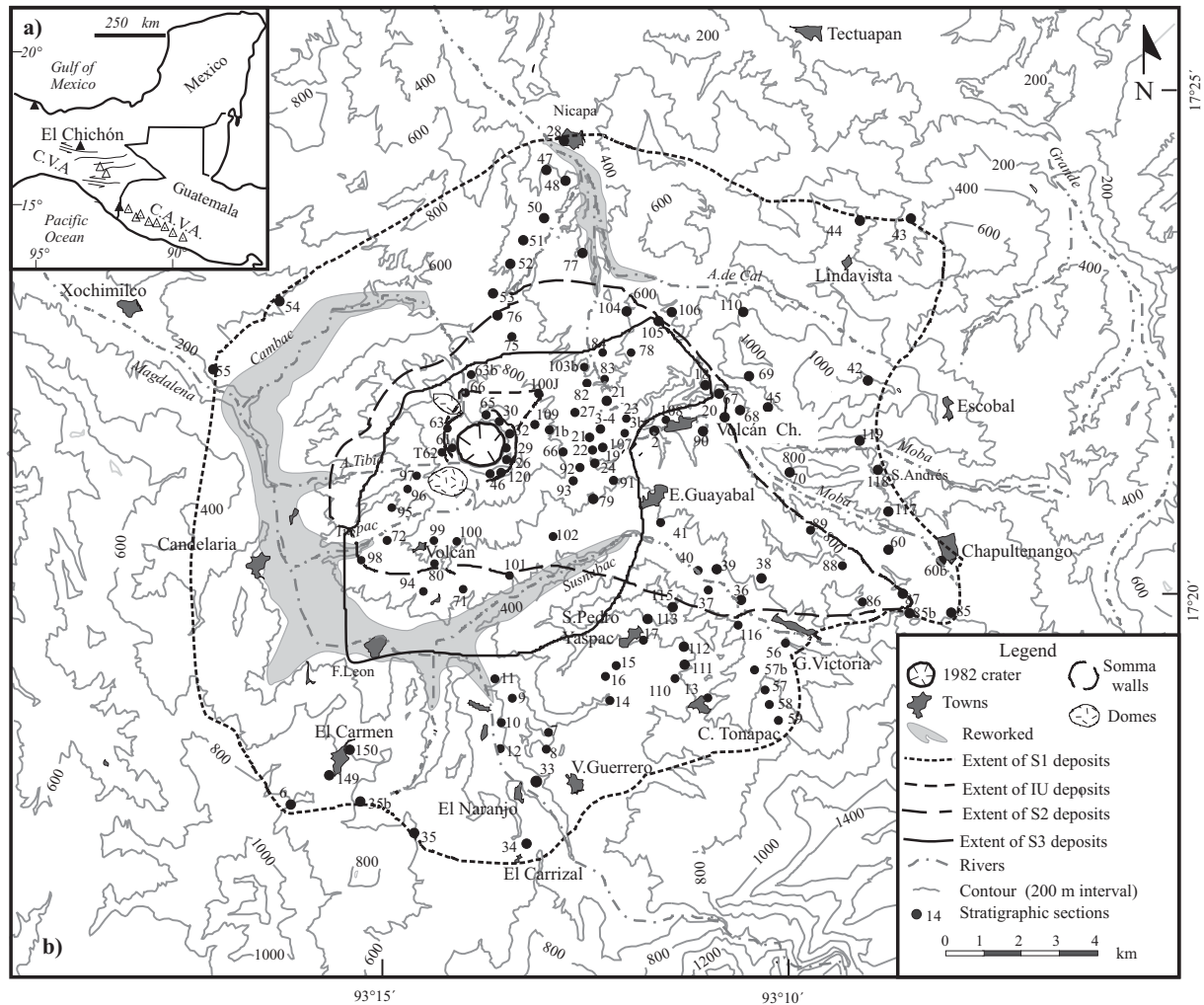


Figure 1. a) Location map of El Chichón volcano in southeastern Mexico. C.V.A.: Chiapanecan Volcanic Arc; C.A.V.A.: Central American Volcanic Arc. b) Distribution of pyroclastic surges S1, S2, IU and S3 determined in this work.

placement of a single flow. A vertical association produced by the emplacement of a single flow has been recognized in both dry surges of hydromagmatic origin (Schmincke *et al.*, 1973; Sohn and Cough, 1989, 1993; Cole and Scarpati, 1993) and blast surges (Fisher *et al.*, 1987; Druitt, 1992; Belousov, 1996), reflecting the vertical and lateral progressive change in both solids concentration inside the clouds and transport mechanism. In these cases, a flow unit generally consists of a fining upward sequence made up of a coarse traction carpet overlain by a finely laminated or cross-stratified layer (Sohn, 1997) and eventually capped by a structureless fine ash (Walker, 1984). Ritchie *et al.* (2002) refers schematically to these layers as *layer I* (or *breccia layer*; Schmincke *et al.*, 1973), *layer II* and *layer III*. Instead, in wet pyroclastic surges emplaced by a three-phase medium (gas + water vapor + solid particles), a flow unit lacks a coarse-grained basal part (Cole, 1991; Hughes, 1995) and can be distinguished from the contiguous units by structural and textural variations. Evidence for a wet emplacement

includes the occurrence of vesicles, accretionary lapilli, syn-depositional slumping, and plastering against vertical objects (Lorenz, 1974; Cough and Sohn, 1990; Dellino *et al.*, 1990; Cole *et al.*, 2001).

In this work, we provide a detailed description of pyroclastic surge units S1, IU, S2, and S3, based on the inspection of 150 stratigraphic sections around the volcano and at variable distances from the vent: proximal (0–3 km), medial (3–5 km) and distal (> 5 km) (Figures 1b and 2). Pyroclastic surge units are composed by varicolored, poorly sorted horizons of fine to medium lapilli, rich in fine ash. These are intercalated with massive to cross-stratified, well sorted horizons of medium to coarse pumice lapilli with minor amounts of medium to fine ash (Figure 3). The variability in these features has been attributed respectively either to their emplacement from diluted pyroclastic density currents rich in condensing water vapor (wet) or in superheated steam (dry) pyroclastic surges (Walker, 1971; Sheridan and Wohletz, 1983; Wohletz, 1983; Fisher

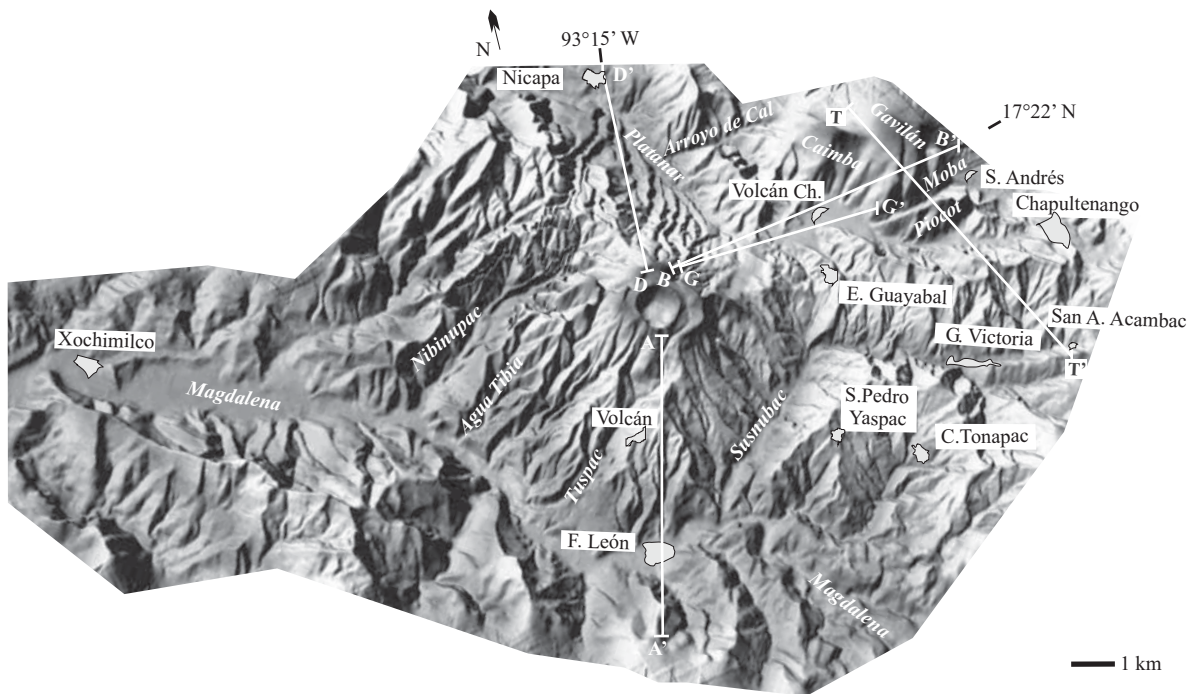


Figure 2. Digital elevation model of El Chichón volcano produced from 1987 aerial photographs of INEGI (Instituto Nacional de Estadística, Geografía e Informática). Map elaborated by GYMSA S.A. de C.V. Main villages and rivers are shown. AA', BB', GG', DD' and TT' are topographic profiles shown in Figures 4 a-d and 10b.

and Schmincke, 1984), although in the case of complex pyroclastic sequences, different fragmentation mechanisms can operate at one time (Cioni *et al.*, 1992; Taddeucci and Palladino, 2002; Dellino *et al.* 2004b), and microscopic investigations of clasts morphology are needed for a precise reconstruction of the eruptive dynamics.

Pyroclastic surge deposit S1

S1 represents the most widespread unit, covering an estimated area of 213 km². It consists of six wet cohesive horizons composed of fine-medium ash interbedded with two dry horizons of medium-coarse lapilli (Figure 3), all of which have a variable distribution around the volcano and merge discontinuously beyond 3.5 km from the crater, where

they are not covered by subsequent deposits (Table 2). Due to the lack of exposures in proximal areas, the lateral facies variations and the relationships between different horizons can be evaluated only in medial-distal areas.

The best S1 sequences occur in the eastern sector of the volcano between 3.6 and 4.7 km mostly below the present ground surface (Figures 4 a-b, 5a-b) or rarely exposed (*e.g.*, section 113). The most complete S1 sequence occurs at 4.8 km to the E of the crater (section 67, Figure 4b), where S1 reaches a maximum thickness of 160 cm. In other sectors (*e.g.*, to the N and S; Figure 4c-d), S1 unit consists of a maximum of four horizons (S1-0, S1-1, S1-2 and S1-3).

The first horizon, S1-0, is red-orange in color due to the abundance of altered lithic fragments from the old dome. It has a N-S elongated distribution reaching a maximum

Table 1. Bed thickness measurements (following Ingram, 1954) and grain size (after Cough and Sohn, 1990).

Bed thickness	cm	Grain size	Diameter (mm)	Φ
Lamina	< 1	Fine ash	< 0.063	> 4
Very thin beds	1 – 3	Medium ash	0.063 – 0.5	1 to 4
Thin beds	3 – 10	Coarse ash	0.5 – 2	1 to -1
Medium beds	10 – 3	Fine lapilli	2 – 4	-1 to -2
Thick beds	3 – 10	Medium lapilli	4 – 16	-2 to -4
Very thick beds	> 100	Coarse lapilli	16 – 64	-4 to -6
		Fine blocks	64 – 256	-6 to -8
		Coarse blocks	> 256	< -8

distance of 6.3 km to the S (Table 2). The overall distribution of S1 unit (Figure 1b) is given by the S1-1 horizon, gray in color, which extends almost radially to the N and W, with a lobate distribution in the eastern and southern sectors, reaching 9.5 km to the NE (section 43), 10.5 km to the ESE (section 85), 9.5 km to the S (section 34), and 4.5 km to the W (section 55).

The horizon S1-3 represents the second most dispersed, and the thickest horizon among all, reaching a maximum thickness of 100 cm at 4.8 km (section 67, Figure 4b), and maximum distances of 5 km N, 4.8 km to the E, and 7.5 km to the S (section 33). It is highly erosive on underlying horizons, particularly near breaks in slope (Figure 4c, Table 2).

Samples from S1 horizons are scattered in the pyro-

clastic surge field in the Inman (1952) diagram (Figure 6a). S1-0 is very poorly sorted and coarser-grained in comparison to other horizons. Very poorly sorted samples (outside the pyroclastic flow field) occur to the N of the crater. This anomalous distribution can be attributed to its high accidental lithic content and the presence of ash aggregates (Table 2), which caused a shift of data points in the pyroclastic flow field. Alternatively, fragments picked from the underlying fallout layers A1-2 may have caused this artificial shifting of the data points, considering the high erosive power of S1-0 in flat areas (Table 2). S1-1 and S1-2, similarly show a great variability of $Md\Phi$ and $\sigma\Phi$ (Figure 6a), with distal-facies samples (between 7.5 and 9.3 km to the SE, and 4.7 km to the E) characteristically finer grained. S1-3 and S1-7 horizons fall within the range of layer 1 (*breccia layer* of

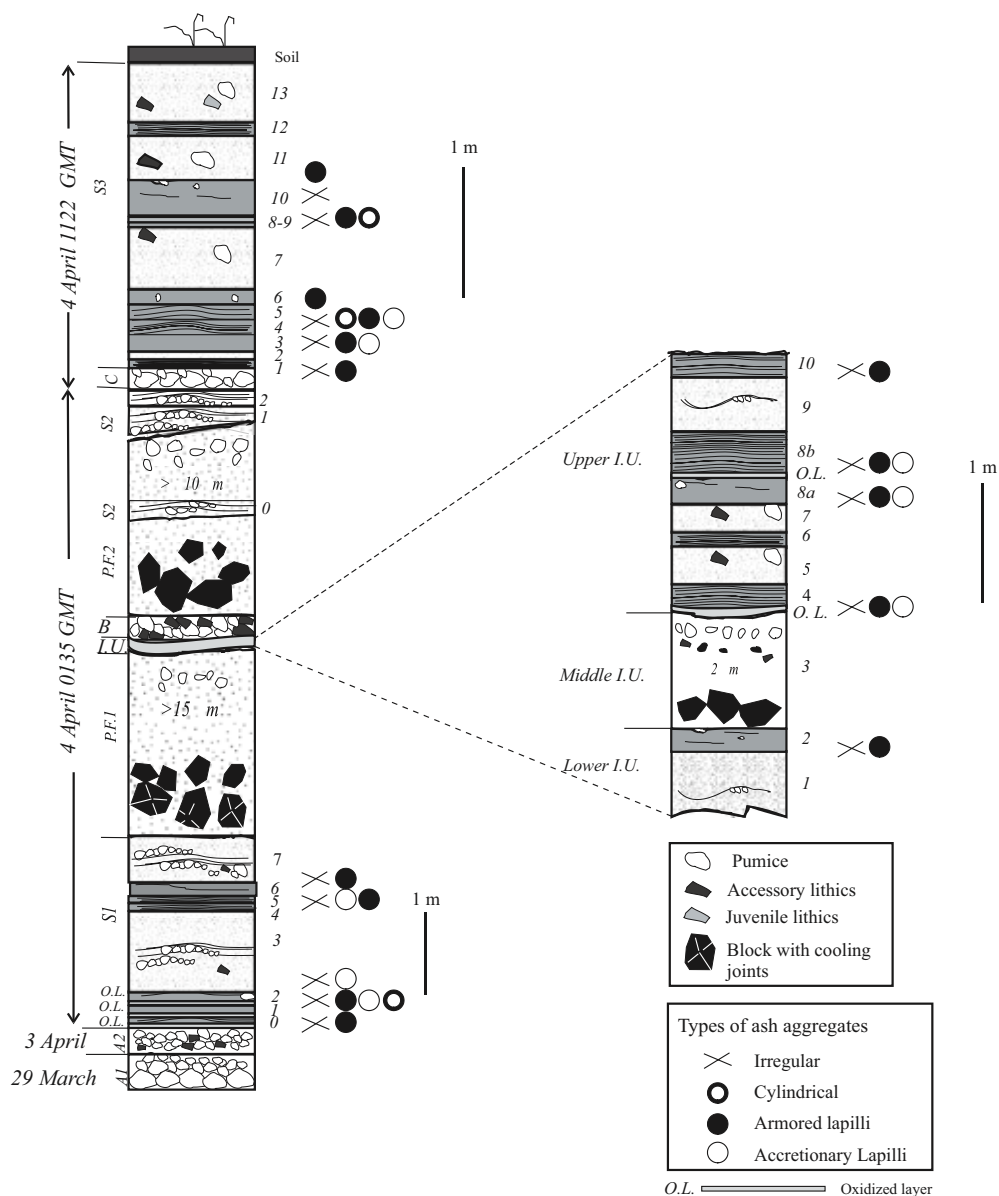


Figure 3. Composite stratigraphic section of the 1982 eruption showing different types of ash aggregates found in wet horizons.

Table 2. Main depositional features of the S1 horizons around the volcano. Numbers in parenthesis refer to stratigraphic sections in Figure 1b. Maximum pumice and lithic clasts are averages on five measurements. All altitudes are given in meters above sea level.

Horizon	Outcrops and thickness	Texture	Structure	Notes
S1-0	<p>N–S elongated distribution up to 6.3 km to the S (10), 5.3 km SE (37) and 3.9 km to the N (52).</p> <p>To the S–SE crops out at distances > 5 km and altitudes between 300 and 500 m, between 7 and 3 cm thick.</p> <p>To the N crops out between 600 and 680 m, at distances >3 km, ranging in thickness between 0.5 cm and 4 cm.</p>	<p>To the S: red to dark-red, slightly cohesive, poorly sorted mixture of medium lapilli-ash, rich in accidental lithics from the old dome (up to 20%). Other components are ash aggregates (up to 30–40 %), white to yellow rounded pumice (30%), crystals (10%; hbl>pl>cpx), juvenile lithics (10–15%).</p> <p>To the N: orange to red poorly sorted mixture of fine-lapilli to medium-ash, with scattered accidental lithics (3–5%). Major components white to yellow rounded pumice (30%), crystals (up to 40%), ash aggregates (10–20%). It rests above a red-oxidized layer and fallout layers A1-2.</p>	<p>Generally structureless. Slightly laminated at altitudes > 460 m, to the S.</p>	<p>Erodes fallout layers A1/2 (9 cm thick at 6.3 km S, and 13 cm at 3.9 km N).</p>
S1-1	<p>To the E, buried by deposits of subsequent activity at altitudes between 500 and 620 m and distances between 3.6 (107) and 4.7 km (90-67). Crops out between 4.9 (20) and 10.5 km (60b). Plastered against topographic highs (30–45°) of Cerro El Gavilán (45 a-d). It ranges in thickness between 2 and 4 cm, reaching a maximum of 10 cm at 500 m (67). Thickest at lower altitudes.</p> <p>To the NE, crops out between 3.5 (104) and 3.7 km (82), thickness between 2 and 4 cm. At 9.5 km (44) laterally discontinuous with a maximum thickness of 3 cm.</p> <p>To the SE, at altitudes between 700 and 560 m and distances of 4.5 (113) 4.7 km (114), thickness between 4 and 8 cm, thickest in topographic lows.</p> <p>To the SSO, crops out discontinuously between 6.5 (12) and 9.5 km (34), thickness between 3.5 and 9 cm; thickest in topographic lows.</p> <p>To the N, crops out between 3.5 (76) and 7.5 km (28), at altitudes between 680 and 320 m. Thickness between 4 and 7 cm, being thickest at lower altitudes.</p> <p>To the W, crops out only at 4.5 km (54) with a thickness of 3 cm.</p>	<p>Dark to light gray cohesive deposit of medium-fine ash and slightly vesiculated. Undulating contact with no exchange of material with the overlying S1-2 horizon. Components: white sub-rounded pumice (max. 2 cm) (20–50%), gray juvenile lithics (10–15%), ash aggregates (2–10%), crystals (10–30%; pl>hbl>cpx).</p> <p>Dark-gray cohesive deposit of fine-medium ash. Laterally discontinuous; in undulating contact with the overlying S1-2 horizon sometimes mixed with it.</p> <p>Light to dark gray, slightly vesiculated deposit of medium-ash with minor lapilli. Major components are white sub-rounded pumice (50%), crystals (40%; pl>hbl>cpx) and juvenile lithics (10%). Ash aggregates (5–10%) occur to the SE (114) and SO (6). At 8.5 km to the SO, S1-1 consists of two distinct layers separated by a red oxidized lamina in undulating contact.</p> <p>Light-gray, wet and cohesive deposit of medium-fine ash with scattered lapilli. In undulating contact with S1-0 and S1-2, through a red oxidized layer, mm-thick.</p> <p>Light-gray deposit of fine-medium ash, consisting mainly of white pumice (60–80%), juvenile lithics (10%) and crystals (20–30%).</p>	<p>Generally structureless. A slight lamination is due to an alternation between beds with different grain sizes or degree of vesiculation.</p> <p>Not observed.</p> <p>Massive at altitudes between 400 and 500 m. Poorly developed lamination due to alternating coarser and finer ash layers at altitudes >680 m.</p>	<p>Always in non-erosive contact with fallouts A1-2 (13 cm thick at 3.7 km) by means of a mm-thick oxidized layer.</p> <p>_____</p> <p>_____</p> <p>In sharp contact with S1-0 or A1-2</p> <p>In sharp contact with 18 cm of fall A1-2.</p>
S1-2	<p>To the E, between 3.7 (3b) and 4.7 km (90) at altitudes between 510 and 610 m, buried by deposits of subsequent activity. Thickness between 2 and 5 cm. Plastered downcurrent of topographic highs (Cerro El Gavilán, section 42). Crops out to the SE, at 700 m and 4.5 km with a maximum thickness of 2 cm.</p> <p>To the N, crops out at 3.5 km (76); large lateral variations in thickness are due to partial erosion by S1-3, and the irregular-non erosive contact with S1-1.</p>	<p>Light-brown fine to medium vesiculated ash, in sharp (90) or undulating contact (3b, 113) with the underlying S1-1 horizon. Components are white subrounded pumice (50–70%), crystals (30–40%), minor juvenile lithics (10–20%) and ash aggregates (5–10%).</p> <p>Dark-brown thin bed of medium-fine ash, composed of sub-rounded white pumice (>50%), juvenile lithics (20%) crystals (pl>hbl>cpx) and ash aggregates (5–10%).</p>	<p>Structureless.</p> <p>Structureless.</p>	<p>_____</p> <p>Partially eroded by S1-3.</p>
S1-3	<p>To the N, crops out between 3.5 (76) and 5 km (50) at altitudes between 700 and 450 m, thickness between 8 (51) and 14 cm (76).</p>	<p>Light-gray to reddish medium-coarse lapilli of rounded pumice (up to 4 cm) hydrothermally altered. Scattered (5–10%) angular accidental lithics (0.7–1 cm).</p>	<p>Plane-parallel stratification in flat topography (e.g., at 3.5 and 3.9 km). Crudely stratified (53) or massive and disorganized (51) on the stoss-sides of a break in slope.</p>	<p>Strongly erosive (up to 4–5 cm) on the underlying horizons, particularly when a break in slope occurs.</p>

Table 2. Continued.

Horizon	Outcrops and thickness	Texture	Structure	Notes
S1-3 (cont.)	To the E, buried by deposits of subsequent activity between 3.6 (107) and 4.7 km (90). Maximum thickness of 100 cm (67) at altitudes of 500 m.	Dry, non-cohesive deposit of light-gray to yellowish medium-coarse rounded pumice lapilli (50–70%), crystals (30–50%) and minor juvenile lithics (10%).	Weak cross-stratified, (stoss sides 3–5°) at 3.7 km E (3b). At 4.7 km composed by symmetrical inverse graded lenses (few cm long) of rounded pumice (18), or normally graded thin beds (67) overlain by plane-parallel stratification and capped by a continuous cm-thick layer of structureless fine ash.	It contains charcoal cm-sized fragments.
	To the SE crops out between 4.5 and 6 km (113-110) at altitudes between 700 and 500 m. Thickness between 12 (113) and 30 cm (114), thickest in topographic lows.	Light-gray to yellowish deposit of medium to coarse pumice lapilli with minor coarse ash. Accidental lithics (6–0.5 cm) from the old dome (10–15%) occur between 5.7 and 7.5 km to the S.	At 4.5 km SE, and altitudes of 700 m (113), consists of plane-parallel thin beds (2 cm) of rounded, inversely graded pumice lapilli overlain by a thin massive bed (2cm) of white, structureless, fine ash.	Erosive on S1-0 and S1-1.
	To the S, crops out between 5.5 (9) and 7.5 (33) km, at altitudes between 480 and 300 m ranging in thickness between 10 (9-11) and 20 cm (33). Thickest in topographic lows.	To the SE (113) a white pumice lapilli bed is covered by a thin red film.	To the S, at altitudes between 400 and 480 m, consists from the base to top of a massive bed (up to 23 cm) of medium-fine pumice lapilli, overlain by a structureless bed (up to 3 cm) of gray to brown fine ash.	At altitudes < 480 m to the S underlies reworked material (up to 10 cm in section 8).
			At 7.5 km (33) at altitudes of 300 m is a medium bed coarse-tail graded (inverse grading of rounded pumice lapilli and normal grading of lithic fragments).	
S1-4	Recognized only at 3.6 and 3.7 km E–SE, between 620 and 560 m, below the present ground surface, thickness between 0.5 and 2 cm.	Medium-fine purple ash consisting of white sub-rounded pumice (50–60%), juvenile lithics (10–20%) and crystals (pl>hbl>cpx).	Multiple mm-thick laminae, different in color and degree of vesiculation.	Laterally discontinuous because eroded by subsequent flows.
S1-5	To the E, buried by subsequent deposits. Discontinuous between 3.6 and 4.7 km (107-67) and altitudes between 620 and 500 m. Crops out altitudes of 700 m at 4.5 km to the SE (113), thickness between 1 and 2 cm.	Dark-pink fine to medium ash with scattered fine-medium lapilli, consisting of white pumice (20–50%) crystals (10–40%), minor juvenile lithics (5–10%) and ash aggregates (2–15%).	To the E: massive, vesiculated thin bed of fine ash in undulating contact with S1-4 at 3.6 km (107); multiple succession of mm-sized laminae in sharp non-erosive contact with S1-3 at 4.7 km and altitude of 500 m (67). At altitudes of 700 m to the SE is a continuous layer of vesiculated fine-ash.	Discontinuous at distances of few tens of meters to the E (e.g., sections 90-67).
S1-6	Discontinuous between 3.6 and 4.7 km E and at 4.5 km SE, overlying S1-5 or S1-3 with a maximum thickness of 8 cm at 500 m	Light-pink to purple vesiculated, medium ash with minor fine-medium lapilli, consisting of white sub-rounded pumice (50–60%), juvenile lithics (10–20%) crystals (5–30%), and ash aggregates (10–15%).		
S1-7	Asymmetrical distribution in the eastern sector between 3.6 and 4.7 km. To the E, below the present ground surface at altitudes between 500 and 620 m, ranging in thickness between 10 cm (90) and 40 cm (107). Marked decrease in thickness with distance from the crater. It crops out at 3.7 km NE (82) at altitudes of 640 m, and the SE at 4.5 km (113) at altitudes of 700 m.	Gray to reddish rounded pumice lapilli (max. 5 cm) and minor coarse ash. Accidental lithics (2–3 cm) from the old dome (5–10%), widely dispersed in the deposit.	At 3.7 km (3b): vertical transition between an inverse graded, pumice rich basal thin bed, to cross-stratified upper portion. Massive deposit in proximity of a 100 m high topographic obstacle (82) to the NE. To the SE (113): vertical transition between a basal bed of fine pumice lapilli (2 cm), overlain by a massive bed (12 cm) of gray coarse ash with scattered fine pumice lapilli.	Lateral variations difficult to follow because the deposit is poorly exposed.

Schmincke *et al.*, 1973) and layer 2. Cohesive horizons (S1-4-5-6) plot in the range of layer 2 (Figure 6a).

Pyroclastic surge deposit IU (Intermediate Unit)

This unit was first described by Macías *et al.* (1997a), and was subdivided in three subunits: Lower, Middle, and Upper. In this work we follow the terminology proposed by previous authors. The overall distribution of the Intermediate Unit is mainly restricted to the moat area between the Somma walls and the 1982 crater, reaching a maximum distance of 1.5 km to the NE (Figure 1b), and covering an area of 3.5 km².

The basal subunit (Lower IU) is exposed in deep canyons running roughly parallel to the Somma crater walls, SSE of the crater where it lies above pyroclastic flow 1 (PF1) with a sharp contact. In this area, it is indurated and consists of an alternation between light-blue ash with thin beds of medium to coarse yellow lapilli. In the WSW sector of the moat, in sections oriented perpendicular to the Somma walls, two horizons can be distinguished (Figure 4e, Table 3).

The Middle IU is in sharp contact with both Basal and Upper IU subunits. It consists of a light-gray block and ash flow deposit (IU-3) with a maximum thickness of 200 cm. The lowermost part crops out solely in the SE sector of the volcano, in canyons oriented subparallel to the Somma walls. It consists of angular juvenile and scattered accessory lithic clasts from the old dome. These clasts are up to 25 cm in diameter and immersed in a scant matrix of light-gray coarse lapilli of the same composition (section 120). The uppermost part is finer grained and consists of yellow, coarse pumice lapilli alternating with fine, hydrothermally altered accessory lithic blocks from the old dome (sections 46, 62, and 30). It crops out in canyons oriented roughly perpendicular to the Somma walls, to the W, S and N of the volcano.

The Upper IU crops out in the moat area (Figure 5c). The contact with the uppermost part of the Medial IU was only recognized where radial gullies of the 1982 crater become deeper than 4 m and intersect the Somma walls to the ESE (section 120-b, Figure 5d) or ENE (section 30) sectors of the volcano. To the NE and NW sectors of the volcano, where the Somma walls are lower or absent, the contact between these subunits is only visible in valleys deeper than 15 m. The most complete exposure of the Upper IU (section 30, Figure 4e) consists of a succession of four wet and three dry surge horizons with a total thickness of 175 cm that overlies the IU-3 horizon (Table 3). In some cases (section 32), none of the Upper IU horizons are clearly distinguishable because they are plastered and intimately mixed against the vertical Somma walls.

Surge horizons from Upper IU (Table 4, Figure 4e) are generally thicker and lack of structures near the crater rim. Stratification occurs between 500 and 600 m from vent

(Table 3, Figure 4e), where wet and cohesive horizons (IU-4, IU-6, IU-8 and IU-10) display a plane parallel stratification consisting of multiple laminae of fine ash, different in color and grain-sizes; dry horizons (IU-5, IU-7, and IU-9) are characterized by poorly to well developed cross-stratification along their entire thickness, or consist of a fining upward sequence of beds displaying different structural features (Figure 4e, Table 3). Most samples of IU are well sorted and fine grained, but massive and cohesive deposits of Lower IU crop out in the W sector (Figure 6b).

Pyroclastic surge deposit S2

The overall distribution of pyroclastic surge deposit S2 determined during this work is asymmetrical and elongated to the SE, where it reaches a maximum extension of 10.5 km from the crater and covers an area of 57.1 km² (Figure 1b). Alternating surge horizons with different textural features were not recognized within this unit. Instead, several successions of surge beds displaying different structural and textural features with respect to distance and azimuth from the crater were observed.

The best exposures of S2 are confined to the E sector of the volcano (Figures 2 and 4a-b) where S2 crops out discontinuously between 1.3 and 4.7 km from the crater (sections 109 and 90, respectively). In this direction, S2 consists of one to several bedsets, made up of a fining upward sequence of two or more layers, which are intercalated to (S2-0) or directly overlie (S2-1, S2-2) pyroclastic flow PF2 (Figures 4a-b, 7 a-b). Up to 3.3 km, these bedsets generally consist of a coarser grained base (20–30 cm) of rounded inversely graded pumice lapilli and blocks overlain by plane parallel thin beds of coarse ash to fine lapilli, and capped by a cm-mm continuous layer of structureless fine ash. Trains of rounded white pumice (up to 10 cm) are draped by smaller pumice clasts, similar to structures observed in fluvial environments, this feature was observed in S2-0 at 3.3 km to the E (section 23).

At distances greater than 3.6 km to the E and NE from the crater, S2 rests with an erosive contact on fallout B (sections 107, 18, 3b, 67, 82, 84; Figures 4a-b, 5a). To the N, S2 crops out on interfluvial up to 2.5 km from the crater, underlying fallout C and overlying pyroclastic flow PF2 (section 75, Figure 4c, Table 4), where it displays plane-parallel to weakly cross-stratified beds. Between 3.6 and 4 km to the NE (sections 82, 84, and 104) and up to 2.8 km to the SE (section 79), S2 consists of two or three fining upward sequences of beds (S2-1, S2-2, S2-3) separated by continuous cm-thick layers of fine ash. To the SSW, along the Tuspac River, (Figures 1b and 2), S2 overlies PF1 at distances between 1.1 and 3 km, at altitudes between 780 and 540 m (sections 97, 96, 95, 72 and 98) and near Volcán village (sections 99, 100 and 80, Figure 4d). In this direction, S2 consists of two distinct bedsets (S2-1 and S2-2), with an inversely graded base and an upper finer-grained

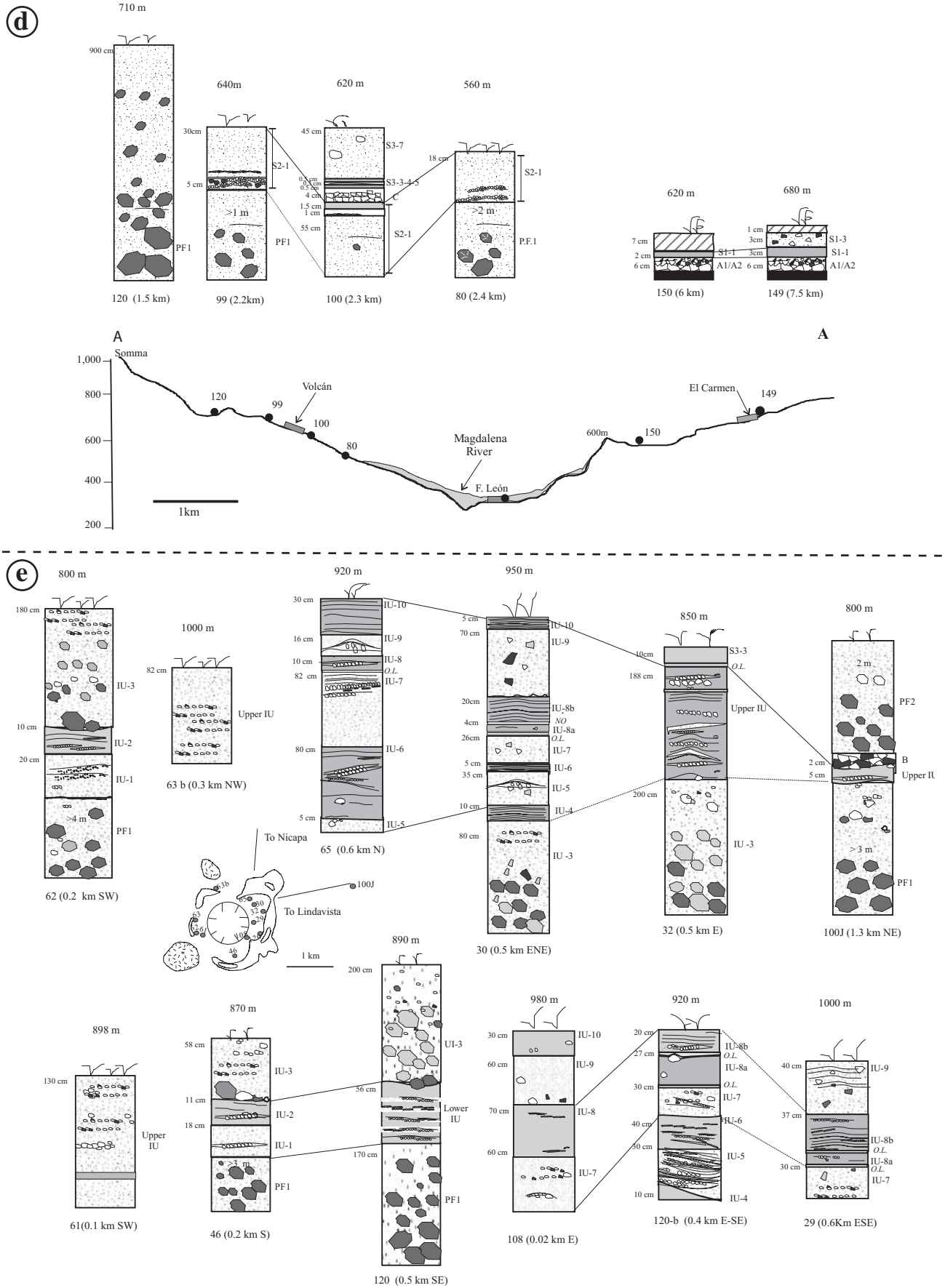


Figure 4. Continued.

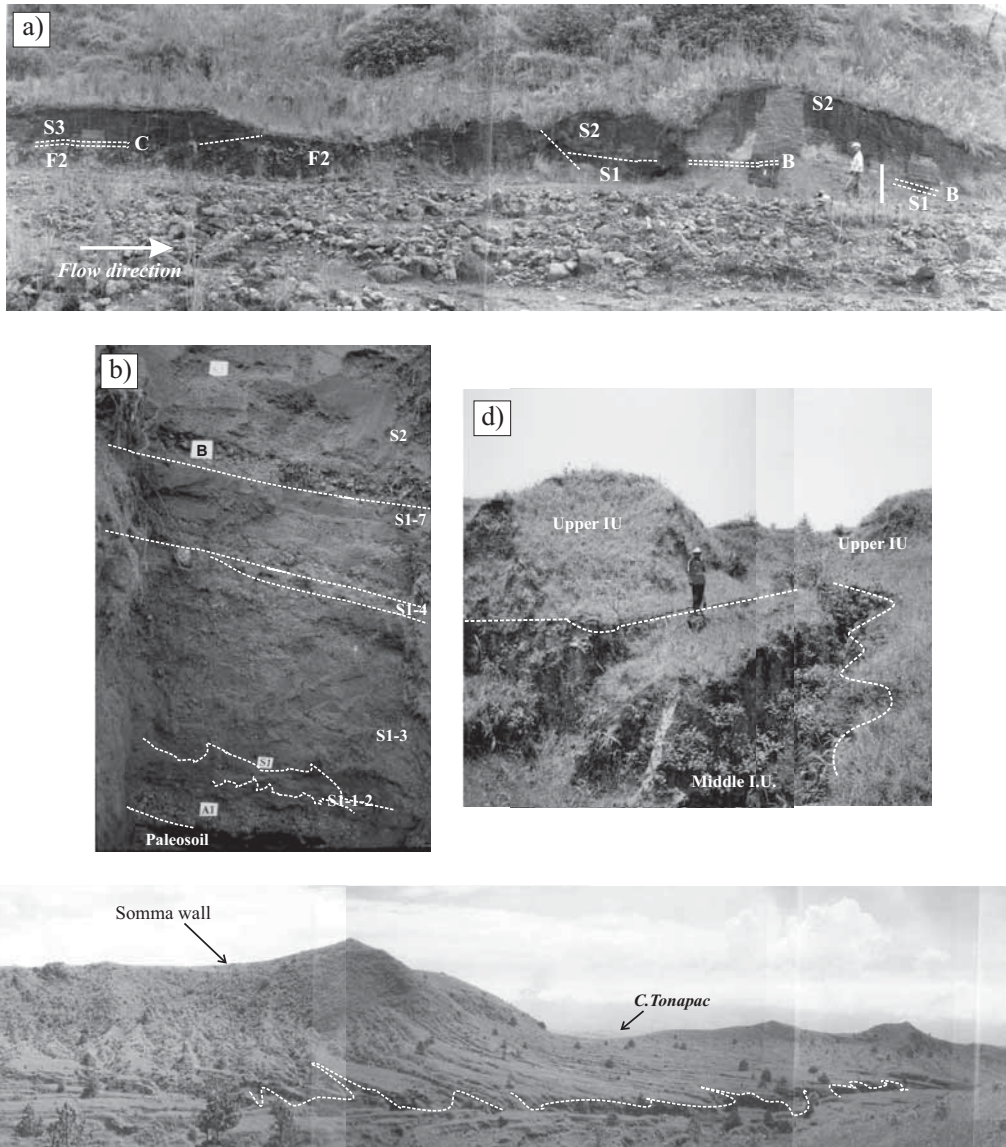


Figure 5. a) Photograph showing the complex relationships existing among different 1982 pyroclastic units at 3.7 km E of the crater. Note the lateral transition between deposits of Phase III (S1, B, S2, PF2) and Phase IV (C, S3). Sandwave structures are evident in unit S2. Unit S1 is almost completely buried by S2 and PF2 deposits. Person is 180 cm high. The white bar on the right side indicates the detail of Figure 5 b. Photograph taken by J.L. Macías in 1994. b) Detail of Figure 5a (section 3b) showing different horizons of pyroclastic surge unit S1. White squares for scale are *ca.* 5x5 cm. c) View looking to SE of the moat area and Somma walls. White dashed line marks the limit between Upper and Middle IU. d) Outcrop at 0.5 km SE in the moat area, showing the contact between Upper and Middle IU (dashed line). Person is 163 cm high.

part with plane-parallel or weakly cross-stratified beds. S2 is more lithic-rich to the S, in comparison to outcrops within the E-NE sector.

Samples from different portions (basal, intermediate and upper) of S2 bedsets, are relatively well sorted and fall in the range of *layer I* and *II* of pyroclastic surge deposits (Figure 6c). Structureless capping fine-ash layers are characteristically poorly sorted and plot in the pyroclastic flow field. This shifting of data may have been probably caused by the incorporation of some clasts from the overlying basal layers of single bedsets or from the overlying fallout C.

Pyroclastic surge deposit S3.

Unit S3 has a NE-SW elongated distribution, and covers an area of *ca.* 44.3 km². The complete succession of horizons can be recognized in channels (1–2 m thick), perpendicular to flow direction (Figure 8). These channels were produced by rain run off during a few hours separating the end of Phase III and the start of Phase IV. In these locations, S3 consists of nine cohesive and varicolored surge horizons of fine and medium ash, interbedded with four dry, gray horizons of medium to coarse lapilli (see Table 4).

S3-3 is the most widespread horizon reaching a maximum of 4.8 km to the E, 4.7 km to the SE, and 4 km to the S. It is a massive red horizon of fine-ash that generally overlies fallout C. In the moat area, it rests on top of Upper IU (sections 46 and 63), and is the only S3 horizon that crops out between 0.6 and 1.5 km from the crater. S3-4 and S3-5 horizons, green and yellow in color respectively (Table 4), consists of cohesive medium-fine ash that overly S3-3 up to 3.7 km to the E (section 3b, Figure 4a) and 3.5 km to the S (section 100, Figure 4d). This vertical succession of horizons typically overlies fallout deposit C at various distances and in different sectors of the volcano.

At 3.6 km to the E (section 107, Figure 4a), no S3 horizons are clearly distinguishable. Unit S3 is strongly erosive on fallout C and consists of a succession of multiple laminae of varicolored fine ash, interbedded with very thin beds of coarse ash to fine lapilli inclined 10° to 15° with respect to the horizontal.

The Inman (1952) parameters for S3 horizons are widely distributed in the field of surge deposits (Figure 6d), except for some samples from varicolored horizons (e.g., S3-4, S3-5, S3-9) that plot in pyroclastic flow field. This

poor sorting of beds probably results from different types of aggregates inside these horizons. The $Md\Phi$ and $\sigma\Phi$ values of S3-3 horizon are widely distributed in the *layer II* field with exception of some samples from distal locations to ESE which are characteristically finer grained (Figure 6d).

ANALYTICAL TECHNIQUES

We analyzed 180 samples representing a variety of horizons within units S1, IU, S2 and S3. Fractions between -4.0 to 3.5Φ were dry, hand sieved, with screens spaced at 0.5Φ interval; fine-grained fractions from 4.0 to 12Φ , were analyzed with a scanning photo-sedimentograph (Analysette 20). All granulometric fractions were washed several times by immersion in an ultrasonic bath with distilled water for approximately 1 minute, and then dried at 60°C . Afterwards, component analyses were carried out with the naked eye or under the binocular microscope, counting between 500 and 800 grains in fractions coarser than 4.0Φ , distinguishing between juvenile and non-juvenile fragments. Juvenile fragments were subdivided into three different classes:

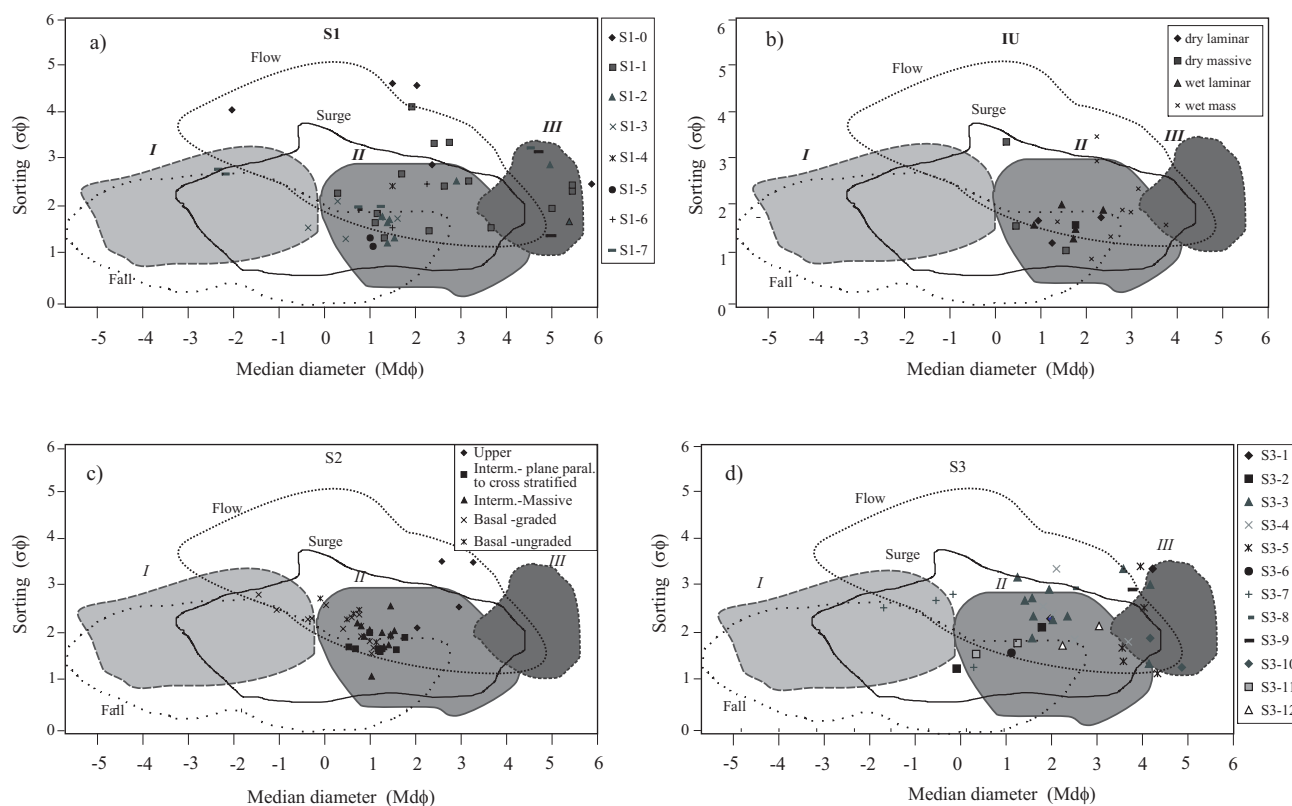


Figure 6. Statistical parameters of Inman (1952), including median diameter ($Md\phi$) and sorting ($\sigma\phi$) for pyroclastic fall, flow and surge deposits in which studied samples of pyroclastic surge units are plotted. Modified from Fisher and Schmincke (1984), Dellino and La Volpe (1995), and Ritchie *et al.* (2002). a) pyroclastic surge S1; b) Lower and Upper IU sub-units; c) flow units of pyroclastic surge S2 in which the coarse basal layer (layer I), the intermediate layer (II), and upper structureless layer (III) are distinguished; d) pyroclastic surge S3. The gray fields marked as I-II and III indicate statistical parameters for coarse basal layers, cross-stratified or plane-parallel intermediate layers and uppermost structureless layers respectively, drawn following the scheme of Crowe and Fisher, (1973) Fisher and Schmincke, (1984), Druitt (1992), and Ritchie *et al.*, (2002).

Table 3. Main depositional features of the Lower and Upper IU horizons around the volcano and at variable distances from the crater. Numbers in parenthesis refer to stratigraphic sections in Figure 1b. Maximum pumice and lithic clasts are averages on five measurements. All altitudes are given in meters above sea level.

Horizon	Outcrops and thickness	Texture	Structure	Notes
IU-1	To the W (62) and S (46), in gullies >9 m, oriented at perpendicular to the Somma walls at altitudes between 870 and 890 m and distances of 500 m from the vent. Thickness between 18 and 20 cm (62 and 46 respectively).	Yellow fine to medium lapilli, consisting of rounded pumice (max 4 cm) and scattered angular accidental lithics (2 cm) from the old dome.	To the W (62) consists of a massive basal portion of rounded pumice lapilli overlaid by weak cross-stratified beds (5–15°) of coarse ash. To the S (62) is a massive thick bed with pumice lenses (10 cm long) overlain by plane-parallel stratified beds	
IU-2	Recognized to the S (46) and W (62), ranging in thickness between 10 (62) and 11 cm (46).	Cohesive, gray to white, coarse-fine ash with minor white rounded pumice lapilli (2–3 cm). Other components are juvenile lithics (15–20%) and crystals (20–40%).	Plane-parallel succession of laminae to the W, massive to the S.	In sharp non-erosive contact with IU-1.
UI-1-2	To the SE (120) in gullies >4 m perpendicular to the Somma walls at 890 m. Thickness between 52 and 62 cm.	Yellow medium-fine pumice rounded lapilli and juvenile sub-angular lithics interbedded with fine-medium light-blue ash.	Plane parallel alternation of very thin beds texturally different.	The deposit is endured.
IU-4	Asymmetric distribution in the eastern sector at distances of 500 m from the crater. It ranges in thickness between 10 (30) and 30 cm (120b, 65). Thicker (30 cm) in small topographic lows to the N (65) and SE (120b) at altitudes between 920 and 930 m.	Cohesive white-blue and gray medium to fine ash, consisting of white sub-rounded pumice (40–50%) angular dense juvenile lithics (20%), crystals (20–50%), and ash aggregates (10–20%).	Massive to the N (65) and SE (120b). Succession of multiple laminae at altitudes >950 m to the NE.	In sharp non-erosive contact with IU-3.
IU-6	In the eastern sector (E–NE–SE) at altitudes between 920 and 950 m (30–65-120b), Thickness between 10 and 40 cm, being thickest in topographic lows.	Non-cohesive deposit of yellow pumice lapilli (3–4 cm) and juvenile sub-angular lithics (2–3 cm).	Massive to the N (65); low angle (5–7°) cross-stratified to the E–NE (30) and S–SE (120b).	Erosive on IU-5.
IU-6	Crops out in the N–NE sector at altitudes between 930 and 950 m (65-30). Thickness between 5 and 80 cm (65); thickest in 3–4 m deep gullies, radial from the crater.	Cohesive deposit of gray to light-blue, medium-fine ash with minor medium-fine lapilli. Components are white sub-rounded pumice (20–60%), juvenile lithics (5–20%) crystals (10–50%) and ash aggregates (5–25%).	Low-angle cross-stratified beds (stoss sides 10–15°) to the N, plane parallel succession of multiple mm-thick laminae to the ENE.	
IU-7	Crops out in the eastern sector (108-120b-30) and to the N (65), at distances from 20 to 500 m, between 920 and 1,000 m. Slight decrease in thickness (40–30 cm) with distance from the crater. It ponds in small topographic lows, reaching a maximum thickness of 80 cm (65).	Non-cohesive yellow pumice lapilli (6–8 cm) and minor coarse-medium ash, with scattered accidental lithics from the old dome (4–6 cm) widely dispersed in the deposit.	Massive near (20 m) the crater rim to the E (108). In topographic lows to the S–SE (120b) consists of alternated coarse and fine-grained beds. To the N is a fining upward sequence made of a massive (60 cm) to inversely graded (12 cm) basal layer of rounded yellow lapilli, overlain by plane-parallel stratified bed (12 cm) of coarse-medium ash.	Overlies IU-6 with an erosive contact (30, 65). Represents the first horizon (section 108) near the crater rim (20 m).
IU-8	Asymmetrical to the E sector at altitudes between 920 (120b) and 1,000 (29) and distances between 20 and 500 m from the crater. Thickness from 12 (65) to 70 cm (108). Decreases in thickness with distance from the crater.	Cohesive deposit of medium to fine light-blue ash, consisting of white sub-angular pumice (30–50%), juvenile lithics (10–20%), crystals (20–60%) and ash aggregates (10–30%).	Is a massive thick bed (70 cm) near the crater rim to the E (108). At distances of 500–600 m to the SSE or ENE (30), consists of a plane-parallel succession of mm-sized laminae with no exchange of material between them (120b), or a thin basal massive portion (7a) and an upper laminated portion (7b), separated by a mm-sized oxidized layer (29-30).	
IU-9	To the N and E at altitudes between 930 and 1,000 m, at distances between 20 and 600 m from the crater. Thickness between 16 and 70 cm; thickest in small topographic depressions (30).	Non-cohesive, yellowish deposit of sub-rounded white pumice (5–6 cm at 20 m; 1 cm at 600 m) with scattered (<10%) accidental angular light-pink lithics from the old dome.	Massive near the crater rim (108); cross-stratified beds with small longitude (20 cm) and low angle (25–30°) at distance of 500 m N (65). Plane-parallel stratification at 600 m ESE (29) and ENE (30).	Overlies IU-8 with an erosive contact.
IU-10	To the E–NE (65-108-30), it crops out at distances between 20 and 600 m from the crater. Thickness between 10 and 30 cm, thickest near the crater rim.	Cohesive deposit of coarse-medium, vesiculated ash with minor lapilli, light-gray to white in color. It consists of white rounded pumice (30–50%), juvenile lithics (20%) and crystals (10–50%; pl>hbl>cpx), and ash aggregates (15–20%).	Close to the crater rim (108) it is structureless. Between 500 and 600 m, is a succession of multiple mm-thick laminae, in sharp, non-erosive contact with each other.	Overlies IU-9 with a sharp non-erosive contact and a mm-sized oxidized lamina.

Table 4. Main depositional features of S3 horizons around the volcano. Numbers in parenthesis refer to stratigraphic sections in Figure 1b. Maximum pumice and lithic clasts refer to an average on five measurements. All altitudes are given in meters above sea level.

Horizon	Outcrops and thickness	Texture	Structure	Notes
S3-1	Crops out only at 2.3 km (1b) and 3.75 km (83) to the E–NE (83) with a maximum thickness of 0.5 cm.	Well-sorted dark-pink to red lamina of fine ash, consisting of white pumice (20–50%) and crystals (30–40%) with minor juvenile lithics (10–15%).	_____	In sharp non-erosive contact with fallout layer C. Laterally eroded by S3-2.
S3-2	Crops out at 2.3 km E (1b) and 3.75 km ENE (83), varying in thickness between 0.5–1 cm.	Light-gray deposit of coarse to medium lapilli with minor coarse to medium ash, consisting of white rounded pumice (20–60%), crystals (30–80%) and juvenile lithics (5–10%).	_____	In erosive contact with S3-1.
S3-3	To the E–NE, crops out between 0.6 and 4.7 km at altitudes between 900 and 510 m, ranging in thickness between 0.5 (83-18) and 13 cm (46). Thickest in proximal areas (46) and progressively thinner far from the crater.	Cohesive brown to red deposit of fine-medium ash, consisting of ash aggregates (50–80%) with minor white sub-rounded pumice (5–10%) and crystals (10–40%). Along the Somma walls ash aggregates are absent.	Generally structureless, characterized by irregular contacts with the upper horizon S3-4. Along the Somma walls displays a weak plane-parallel stratification.	In sharp non-erosive contact with S3-2 in topographic lows to the E–NE (1b, 83). Generally represents the first horizon above fall C.
S3-3	To the S, crops out between 2.3 (100) and 3.5 (71), ranging in thickness between 0.5 and 4 cm, thickest in topographic lows. To the N, observed at distance up to 2.5 km (75b).	Cohesive orange to red deposit of fine-medium ash with minor lapilli consisting of white sub-rounded pumice (50–60%) and crystals (40–50%; pl>hbl>qtz>cpx). Ash aggregates were found at 2.3 km S (15%).	_____	To the S, in contact with F1 and fall C.
S3-4	Crops out to the E–NE between 2.3 (1b) and 4 km (105), ranging in thickness between 2–4 cm. To the S, crops out between 2.3 (100) and 3.5 km (71) at altitudes between 620 and 420 m, being thickest in topographic lows.	Cohesive, vesiculated, light to dark green deposit of fine to medium ash, with minor lapilli. It consists of white rounded pumice (30–60%), crystals (20–70%) and juvenile lithics (10–20%). Ash aggregates (10–20%) occur to the E–NE.	Laminar succession of very thin beds characterized by slight differences in the degree of vesiculation and grain-sizes, up to 2.3 km E. Generally structureless.	Undulating, non erosive contact with S3-3 and S3-5 horizons.
S3-5	Crops out between 2.3 km (1b) and 3.7 km E with a maximum thickness of 4.5 cm, inside small topographic lows. To the S, crops out between 2.3 and 3.5 km (100-71), ranging in thickness between 0.5 and 6 cm, being thickest in topographic lows.	Well-sorted yellow fine ash with minor coarse ash. Main components are white pumice (30–40%) and crystals (70–20%). Ash aggregates (5%) occur to the E and S at 2.3 km (<9%).	Plane-parallel succession of mm-thick laminae, characterized by slight differences in color and degree of vesiculation at 2.3 km E. Generally structureless, locally plane-parallel laminae are visible.	Irregular, non erosive contact with the underlying S3-4 horizon.
S3-6	Crops out only at 2.3 km E, in a small channel (2 m deep) with a thickness of 4 cm.	Vesiculated bed of brown ash made of pumice (20–60%), crystals (40–80%) and minor juvenile lithics (4–10%).	_____	Laterally eroded by S3-6.
S3-7	To the E, crops out between 2.2 (1) and 4.7 km (67) ranging in thickness, between 4 (67) and 20cm (1b). To the S, crops out between 2.3 (100) and 3.5 (71) km, ranging in thickness between 30 and 45 cm, being thickest in topographic lows.	Gray, non cohesive, medium-thick bed of coarse lapilli, consisting of sub-rounded white and gray pumice (20–60%), juvenile lithics (10–30%) and crystals (10–40%).	In proximal zones consists of a basal thin bed of rounded, inverse graded lapilli, overlain by a massive thick bed of coarse ash. Plane-parallel stratification occurs in medial-distal zones (e.g., 4.7 km). Massive in proximity of topographic lows.	_____
S3-8	Both horizons crop out discontinuously between 2.3 and 3.2 km E (1b-3) in small topographic depressions, ranging in thickness between 1 mm and 2 cm.	Both horizons consists of cohesive fine ash different in color: S3-7 is green, S3-8 is yellow, consisting mainly of sub-rounded pumice fragments (40–70%) and crystals (30–60% pl>hbl>cpx). Ash aggregates (10–20%) occur at 3.2 km.	_____	S3-9 overlies with a sharp non-erosive contact S3-8.
S3-10	Crops out between 2.3 (1b) and 4.7 km (67) E and at 3.75 km ENE (83). It range in thickness between 1 cm (67) and 30 cm (1b), being thickest in proximal zones and inside small topographic depressions.	Cohesive, pink deposit of fine-medium ash, consisting of white sub-angular pumice (10–50) and crystals (40–80%).	Generally structureless, but at 3.2 km where it consists of a plane-parallel close alternation of laminae, slightly different in color and grain-size.	_____

Table 4. Continued

Horizon	Outcrops and thickness	Texture	Structure	Notes
S3-11	Crops out between 2.3 (1b) and 3.25 km E (4), at 3.75 km NE (83) and 3.5 km S (71). Major variations in thickness occur to the E at distances of a few meters (e.g. between 22 and 100 cm (3-4).	Light-gray deposit of coarse lapilli and medium pumice blocks (10 cm).	Alternating coarse and fine layers, in small topographic lows in proximal zones (up to 2.3 km) to the E. Sandwave structures (longitude 120 cm, amplitude 20 cm) in medial zones to the E (3.2 km). Massive in proximity of small topographic obstacles (83) to the ENE.	_____
S3-12	Crops out between 2.3 (1b) and 3.25 km (3b) E, and 3.75 km ENE. It ranges in thickness between 0.5 and 6 cm, being thickest in proximal zones and small topographic depressions.	Cohesive light brown deposit of medium-fine ash, mainly consisting of subrounded white pumice (50–60%) and crystals 30–40%.	Structureless in sharp non-erosive contact with S3-11, partially eroded by S3-13.	_____
S3-13	Crops out between 2.3 (1b) and 3.25 km (4) E and 3.75 (83) NE. To the E, range in thickness between 40 and 110 cm, at distance of 5 m (3-4). To the NE is 16 cm thick.	Dark-gray deposit of medium-coarse lapilli, composed of rounded pumice (10 cm) and juvenile lithics (3 cm). Scattered (<5%) accidental lithics (1–2 cm) from the old dome, occur at 3.25 km E.	Massive in small topographic lows (1b). Coarse and fine alternating layers occur at 3.2 km E.	

glass fragments (vesiculated or dense particles), crystals (mainly plagioclase, hornblende, pyroxene, and minor sphene), and different types of ash aggregates (formed by glass and crystals). Non-juvenile components include hydrothermally altered and fractured lithic fragments, with colors varying from light pink to dark red. To investigate the eruptive dynamics (Dellino *et al.*, 1990; Zimanowski *et al.*, 1991; Büttner *et al.*, 1999), grain-sizes between 3 and 4 Φ of selected samples from wet and dry horizons of different units were analyzed under the SEM.

SEM OBSERVATIONS

Almost all varicolored horizons contain ash aggregates with different shapes and internal structure (Figure 3), these are absent in dry surge horizons (Scolamacchia *et al.*, in press). A clear difference exists between wet and dry S1 horizons for grain-sizes between 125 and 63 μm . In these horizons, low vesiculated glass fragments with equilateral sizes crossing at low angles (*blocky shapes*, Heiken and Wohletz, 1985) are dominant. However, glass particles in wet horizons are characterized by the presence of irregular, dendritic fractures on their surfaces. Low vesiculated particles have already been described as one of the features suggesting hydromagmatic fragmentation (Sheridan and Wohletz, 1983; Heiken and Wohletz, 1985; Büttner *et al.*, 1999); irregular fractures on glass were experimentally obtained when hot already fragmented melt entered in contact with excess water (Büttner *et al.*, 1999), indicating a further quenching of particles occurring in wet surge deposits.

In some cases (S1-1 and S1-2 horizons), a μm -thick film enveloped the glass fragments. This film is depleted in alkalis with respect to the fresh glass surfaces and is

characterized by an increase in Al and Fe contents. This feature was not observed in particles from dry horizons. This depletion has already been described as the result of an extreme alteration caused by acid fluids on glass fragments during transport and deposition (Dellino and La Volpe, 1995; Dellino *et al.*, 2001; Büttner *et al.*, 2002). Samples from laminated and sand wave beds of different S2 bedsets show beside glass fragments with blocky shapes (up to 40 wt.% of the total abundance of components), a high percentage of highly vesiculated fragments (20–30 wt. %) in some situations (*e.g.*, S2-1 between 3.6 and 4.7 km E). These abundances suggest that distinct fragmentation mechanisms may have operated at the same time. Great differences also occur in horizons from S3 unit. In particular, both crystals and glass fragments of S3-3 are characterized by a high degree of alteration on their surfaces. Peculiar structures were observed in fractions <63 μm in S3-5, consisting of rounded vesiculated fragments “glued” with crystals (mostly plagioclase). These features give information on the transport medium instead of fragmentation mechanisms. In fact, this fragile structure would have been destroyed by the frequent impacts occurring in a concentrated medium moving at high velocities. Thus, their preservation was guaranteed by a cohesive medium of transport.

DISCUSSION

Eruptive mechanisms of the 1982 pyroclastic surges

The 1982 eruption of El Chichón consisted of four major eruptive phases that occurred between March 29 and April 4, 1982 (Sigurdsson *et al.*, 1984; Macías *et al.*, 1997a). The first two phases occurred on March 28 at 11:32

local time (March 29, 05:32 GMT) and April 3 at 02:30 (April 3, 08:30 GMT) producing two fallout layers. The most catastrophic eruptive episodes occurred on April 4. The detailed revision of the stratigraphy and the component analyses outlined in the previous pages allows to better characterize the succession of events that occurred on April 4, 1982 (Phases III and IV of Macías *et al.*, 1997a), which were responsible for the deposition of pyroclastic surge units S1, IU, S2, and S3.

Previous studies (Sigurdsson *et al.*, 1984, 1987; Macías *et al.*, 1997a) indicate that Phase III of the eruption started at 01:35 GMT on April 4, 1982 (SEAN, 1982) with phreatomagmatic explosions that destroyed the remaining parts of the 1982 dome, and produced the pyroclastic surge S1. However, interpretations offered by these authors on the origin of these pyroclastic surge units are contradictory. They invoke either deposition from diluted clouds of fine-grained material elutriated from pyroclastic flows that were mainly dispersed on the SW flanks of the volcano (Sigurdsson *et al.*, 1984), or the deposition from turbulent clouds generated from hydromagmatic explosions, with temperatures well above 100°C, that were dispersed mainly to the S (Sigurdsson *et al.*, 1987; Macías 1994). This asymmetrical distribution was attributed to a directed explosion in this particular sector (Macías *et al.*, 1997a).

The succession of deposits that become exposed during the last twenty years, indicates that pyroclastic surge unit S1 resulted from eight distinct eruptive events, each triggered by the interaction between ground water and magma and, in most cases, involving the participation of the active hydrothermal system (Casadevall *et al.*, 1984; Rye *et al.*, 1984; Scolamacchia *et al.*, in press). The first eruptive event

produced S1-0, a cohesive horizon red in color, elongated in a N–S direction, that reaches distances of 6.3 km to the S and 4 km to the N (Table 2). The poorly sorted nature of S1-0, as well as its grain size and the high content of accidental hydrothermalized lithics, supports the previous hypothesis (Macías *et al.*, 1997a) suggesting that the first explosions contributed to destroy parts of the remaining dome. Considering the textural and structural features of the deposit (Table 2), as well as the occurrence of peculiar types of ash aggregates (Scolamacchia *et al.*, in press) and clasts morphology, a directed explosion seems unlikely. In fact, the erosive capacity of these pyroclastic density currents on fallouts A1/2 was similar in both directions (reaching a maximum of 4 cm to the N (Table 2) with no evidence of strong erosion in one direction as reported for direct explosions at other volcanoes (Lipmann and Mollineaux, 1981; Fisher *et al.*, 1987). The N–S elongated distribution displayed by this horizon was likely influenced by the topography (see next section). A violent hydromagmatic event characterized by a high water/magma ratio (wet surge type) seems in this case the most likely eruptive mechanism. We believe that Phase III of the eruption began when magma rising in a fractured conduit (weakened by previous activity) entered in contact with the active hydrothermal system (Casadevall *et al.*, 1984). This interaction determined a highly energetic explosion (*flashing*) capable to destroy the remnant parts of the dome, and allowing groundwater to enter in contact with magma. As a result, a pyroclastic density current rich in coarse, hydrothermally-altered fragments and condensing water vapor was produced depositing S1-0 horizon. Significant quantities of groundwater were therefore able to enter in the conduit, producing diluted clouds rich in

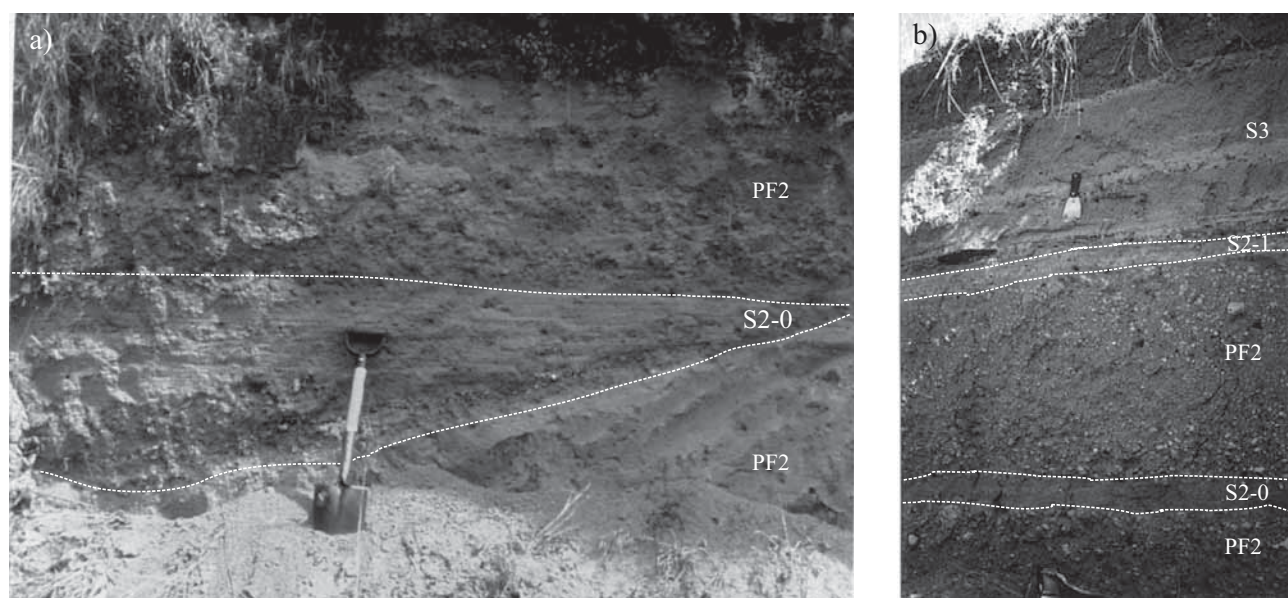


Figure 7. a) Photograph of S2-0 at section 19 located at a distance of 2.9 km to the E. Flow direction is from left to right. Note the erosive contact on PF2, the coarse inversely-graded basal part and the upper portion of S2-0 with plane parallel stratification. Shovel is 67 cm long. b) Section 4 at distance of 3.25 km to the E. Flow direction is from right to left. Spatula is 20 cm long.

abundant water vapor and acid fluids (S1-1 and S1-2).

Depositional features such as the irregular contacts between beds produced by the load of cohesive deposits on plastic deposits beneath, the amount of vesicles (Lorenz, 1974; Dellino *et al.*, 1990), the plastering against steep walls (Sohn and Cough, 1992; Cole *et al.*, 2001), and the absence of a coarse-grained base (Hughes, 1995), together with the presence of four different types of ash aggregates (Scolamacchia *et al.*, in press), and the morphology of juvenile clasts, all indicate that eruptive clouds were rich in droplets of condensing water vapor and/or acid fluids from an active hydrothermal system. These evidences indicate that the water/magma ratio during these events was high (Wohletz, 1983; Zimanowski *et al.*, 1991) and the explosions less energetic (Sheridan and Wohletz, 1983; Büttner *et al.*, 2002).

The availability of water entering in contact with magma was reduced thereafter, determining a high energetic eruptive event. The resulting flow S1-3 was mainly dispersed to the E-NE and capable of carbonizing wood fragments and eroding previous deposits especially in flat areas (e.g. up to 4 km N, Figure 4c).

Afterwards, relatively cold and poorly expanded clouds were generated when great quantities of water gained access to the conduit (e.g., S1-4, S1-5 and S1-6). Instead, for lower amounts of water ($W/M \approx 0.02-0.03$ by mass, Zimanowski *et al.*, 1997), highly energetic episodes produced turbulent hot clouds capable of charring wood (S1-7). This alternating activity might reflect a heterogeneous arrangement of fractures at the crater conduit.

These events caused the removal of the pre-existing dome and decompression of the magmatic system with the subsequent acceleration of the magma through the conduit and the formation of dense pyroclastic currents (PF1) that traveled in deep gullies around the cone (Sigurdsson *et al.*, 1984; Macías *et al.*, 1997a). A pulsating activity that

involved different proportions between water and magma (Lower IU) occurred shortly after the emplacement of PF1, when rising magma entered in contact with ground water. These eruptive events produced small, poorly expanded pyroclastic density currents that remain confined inside the Somma crater. The activity continued producing a small volume pyroclastic flow (UI-3) that was blocked by the Somma walls. It was followed by a close succession of nine hydromagmatic events (Upper IU) that produced poorly expanded clouds. These flows were mainly contained by the Somma walls reaching a maximum distance of 1.5 km to the NE (Figure 4e). The types of ash aggregates found in wet pyroclastic surge deposits of Upper IU and the degree of alteration of juvenile fragments in the dry surge deposits (Scolamacchia *et al.*, in press), indicate the involvement of the hydrothermal system during these eruptive episodes.

At the climax of the eruption, a Plinian column was established which dispersed a lithic-rich fallout layer (B) mainly to the E (Figure 9, Sigurdsson *et al.*, 1984; Carey and Sigurdsson, 1986). Its collapse generated a pyroclastic flow (PF2) that was channeled through major valleys to the ENE (Platanar and Nicapa, Figure 2) following the hydrologic network. Previous studies indicated that pyroclastic surge unit S2 was associated with the emplacement of PF2, consisting of three ground surge deposits underlying respectively three pyroclastic flow units, and an ash cloud surge covering the uppermost part of PF2 (Sigurdsson *et al.* 1984). Nevertheless, S2 extends radially around the crater (Sigurdsson *et al.*, 1984; 1987; Macías *et al.*, 1997a). Sandwave structures were reported in all deposits, but no lateral or distal transitions between ground surge and pyroclastic flow were observed. Instead, PF2 deposits pinch-out against topographic highs where ground surge layers and ash cloud surge layers merge at the flow front.

As described above, one of the most striking features of pyroclastic surges associated with the emplacement of a

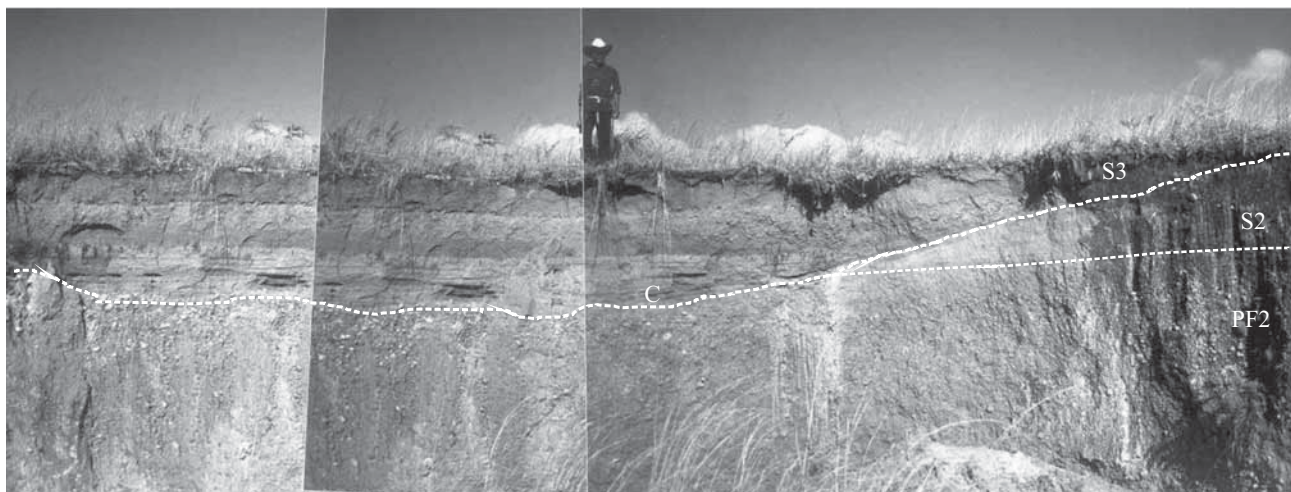


Figure 8. Photograph of section 1b, 2.3 km East from the crater, taken in the direction of flow. Person is 163 cm high.

pyroclastic flow, both at its base (ground surge) and at its top (ash-cloud surge) is their distribution that roughly reflects the distribution of the parent flow. Considering the radial distribution of S2 around the vent, its association with the emplacement of the PF2 seems unlikely. S2 unit was rather emitted directly from the vent and produced independent pyroclastic density currents. Several lines of evidence support an independent origin of pyroclastic surge S2 from pyroclastic flow PF2. S2 is prevalently distributed in the E sector of the volcano, similarly to the other pyroclastic surge units, but it is elongated to the SE up to 10.5 km following the turn of Susnubac River (section 85b, Figure 1b), where it consists of a thin bed of fine lapilli, between fallout B and C. Between 1.3 and 4.8 km to the E of the volcano, one to four successions of beds that become progressively finer from bottom to top were recognized. They invariably have: a coarse base (well to poorly sorted) that can be massive, inversely or normally graded, symmetrically or multiple inversely graded (Figures 4a-b, 7a); an intermediate finer-grained portion, sometimes weakly cross-stratified at low angles ($<15^\circ$) with plane parallel bedding (Figure 7b) or massive; and an upper layer of structureless continuous fine ash. This vertical association has been recognized in pyroclastic surge deposits directly emitted from the vent both as the result of directed explosions (Fisher *et al.*, 1987; Fisher, 1990; Druitt, 1992; Belousov, 1996) or radially expanding clouds associated with hydromagmatic explosions (Sohn and Cough, 1989; Lajoie *et al.*, 1989; Sohn and Cough, 1993; Cole and Scarpati, 1993; Dellino *et al.*, 2004a), and interpreted as deposition from different portions of a single flow. *Cluster bedforms* (Laronne and

Carson, 1976; Brayshaw, 1984) of S2-0 found below PF2 at 3.3 km from the crater, provide an additional evidence for its independent origin. Trains of smaller clasts both upcurrent and downcurrent of a larger one were first described by Hughes (1995) in base surge deposits of Laacher See volcano (Upper Laacher See Tephra). There, they typically occur in the basal and coarser portion of dry surge deposits (*breccia layer* of Schmincke *et al.*, 1973 or *layer I* of Ritchie *et al.*, 2002), and are comparable to cluster bedforms found in fluvial environments.

Juvenile glass in selected samples from different flow units (S2-0 to 3), displays features typical of hydromagmatic fragmentation (like *blocky shapes*, Heiken and Wohletz, 1985; Büttner *et al.*, 1999), but in some cases, up to 30% of highly vesiculated glass is also present.

Therefore, we believe that a contemporaneous phreatomagmatic activity took place during the collapse of the eruptive column that produced fallout B, from a different conduit generating an independent and diluted current (S2-0). Its deposits are well preserved in flat areas to the E, intercalated with PF2. This situation persisted after the deposition of pyroclastic flow PF2, when at least two independent flows (S2-1 and S2-2) were radially dispersed around the crater. These flows were highly erosive in flat areas (to the E) and on topographic slopes to the SSW. This activity marked the end of Phase III, as indicated by a relatively widespread erosive surface on top of S2 and PF2, produced by rain-runoff on fresh deposits, and by a 5 cm-thick layer of reworked material in topographic lows.

Phase IV began few hours later (11:30 GMT; SEAN, 1982) on April 4 with a 29 km high Plinian column (Carey and Sigurdsson, 1986) that produced a normally graded white pumice fallout (C) with a dispersal axis towards the ENE. Pyroclastic surge S3 was deposited afterwards. Sigurdsson *et al.* (1984, 1987) stated that pyroclastic unit S3 consisted of two layers of red to gray pumice rich fine ash, that remains unstudied because it was eroded by heavy rain. Macías *et al.* (1997a) recognized S3 up to 3.5 km from the volcano where it occurs as an alternating sequence of gray to pink cohesive ash, and dune-bedded gray coarse ash overlying pyroclastic flow PF2 in the moat area, and in erosive contact with fallout C at the Somma flanks. These authors attributed its deposition to phreatomagmatic activity. Here, we recognized that unit S3 consists of eight varicolored cohesive horizons composed mainly of fine ash interbedded with four dry surge horizons of gray, medium to coarse lapilli, most of which are only preserved in 1–2 m deep channels.

Field evidences and component analyses evidenced that following the deposition of fallout C, phreatomagmatic activity was dominant. At the beginning, a small pulsating activity produced short-lived currents that traveled few kilometers from the crater and deposited S3-1 and S3-2 horizons, poorly preserved in topographic lows to the E. The following event had a larger magnitude and produced the most widespread horizon (S3-3) which was deposited

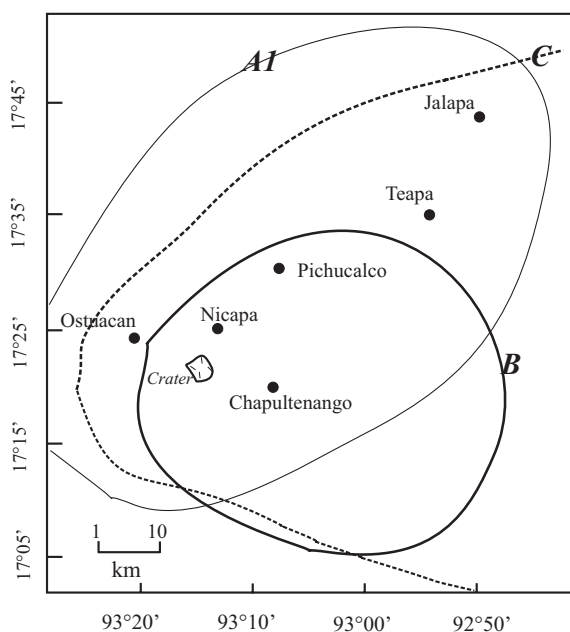


Figure 9. Schematic map showing the 5-mm isopach of fallout deposits A1, B and C as determined by Carey and Sigurdsson (1986).

mainly on the E sector up to 4.7 km from the vent. These eruptive clouds were highly erosive up to 1.5 km to the east as indicated by the absence of fallout C and S3-1 and S3-2 horizons. The large amount of irregular-shaped aggregates with a red Fe-rich film coating (Scolamacchia *et al.*, in press), and the strong alteration of juvenile clasts in this horizon suggest that fluids from the hydrothermal system were involved. The subsequent events (S3-4-5) reached up to 3.7 km to the E and S of the crater; some were short-lived and simply ponded in topographic depressions (S3-6) up to 2.3 km. A larger proportion of water was involved during these three eruptive events as indicated by field evidences like convolute laminations and vesiculated beds (Lorenz, 1974). Therefore, the quantities of water that gained access to the conduit decreased due to temporary unavailability of groundwater or closing of feeding fractures. As a result, a highly expanded erosive current (S3-7), capable of charring wood, was produced. The eruption continued until the end of Phase IV with alternating poorly expanded, relatively cold clouds (S3-8-9-10-12), whose deposits, otherwise eroded, were mostly preserved in topographic lows to the E, and highly expanded hot clouds (S3-11-13) with a high erosive power. Less energetic phreatomagmatic eruptive events occurred during the last stages of Phase IV or during the following days (Macías, 1994). These events produced pyroclastic surges S4 and S5 whose emplacement was confined inside the crater.

The presence of three small inner craters inside the 1 km wide 1982 crater, observed in photographs shortly after the eruption, suggests the existence of a multiple-conduit feeding system. Thus, magmatic and phreatomagmatic activity likely took place at the same time. In this context, fluids from the active hydrothermal system were variably involved in different proportions during the eruptive events.

Interaction with the topography and depositional structures of pyroclastic surges

Studies of pyroclastic surges elsewhere have pointed out the influence of topographic obstacles on the flow behavior of pyroclastic surges (Fisher *et al.*, 1987; Sohn and Cough, 1989; Cough and Sohn, 1990; Druitt, 1992; Cole and Scarpati, 1993). Notwithstanding the overall dilute nature of these currents (solid content of 0.1–1 vol %; Wilson and Houghton, 2000) with respect to pyroclastic flows, they are considered density-stratified (Valentine, 1987). Fisher (1990) pointed out that the *transport system* of such kind of density current is different from the *depositional system*. This means that the structural and textural features of the deposits only reflect processes that acted during the last stages of deposition and are greatly influenced by the local topography, as well as by the material provided from the upper portions of the clouds (transport system).

The analysis of the facies variations in the 1982 pyroclastic surges with distance from the vent and the

topographic conditions, allows to determine the potential flow trajectories and the pathways of currents in a future eruption.

Main topographic irregularities occur at different distances from the crater (Figure 2), and are related to ancient volcanic structures (Somma crater) and to regional folds and faults systems (García-Palomo *et al.*, 2004). These topographic irregularities influenced the distribution pattern of different types of flows in a radius between 0.5–1 km, and at 3.7–4 km from the vent.

The distribution of surge deposits at El Chichón indicates that the 1,100 m Somma walls were able to control the distribution of small pyroclastic density currents (IU horizons), at least to the SE, but not to the NE, where they reach 900 m in height. Lateral facies variations displayed by the Lower and Upper IU horizons in the moat area (Table 3), suggest a progressive dilution of flows at distances of few hundred meters, as noted by Sohn y Cough (1989) in small-sized volcanoes.

The best exposures of all pyroclastic surge units occur to the E of the volcano (Figures 1b, 4 a-b), reflecting the presence of the San Juan Fault that runs from the Grande River to the E, for 16 km across the volcano to the Xochimilco village to the W (García-Palomo *et al.*, 2004). The smooth topography in this direction greatly contributed to the acceleration of the flows and, consequently, to an increase in their momentum (mass x velocity). This is underscored by depositional features of pyroclastic surge deposits S2 and S3 at distances between 1.3 and 1.7 km from the vent (Figures 4a-b). Two flow units of pyroclastic surge S2 at 810 m (S2-0 and S2-1, section 109, Figure 4b) show strong traction conditions during transport (*e.g.*, basal part of S2-0 is cross-stratified) with a continuous feeding from the upper portion of the cloud (poorly sorted beds overlain by a massive one) or waxing pulsating traction during transport and deposition (*e.g.*, succession of stacked inverse beds in the basal portion of S2-1) followed by a mechanism of traction *sensu strictu* (cross-stratified upper portion of S2-1) (Sohn, 1997). In a similar way, S3-3 was highly erosive up to 1.5 km from the vent (Figure 4a). All these features indicate that the currents were accelerating and concentrated. Small variations in the topographic gradient even of a few degrees (*e.g.*, at 1.7 km in section 27, Figure 4b), destabilized and decelerated the flows. Under these fluctuating conditions, the flows dropped their coarser load (symmetrical reversely graded coarser base in S2-1) (Middleton, 1967) and most of their fine grained load instantaneously (upper massive and disorganized portion). Depositional features of pyroclastic surges S2 and S3 at 2.3 km (Figures 4a, 8), show the importance of small topographic depressions on flow behavior (ponding). In fact, although the general topographic conditions at this distance favored flow expansion, as evidenced by cross-stratification in S2 (Figures 4a, 8), a deceleration occurred in small channels produced by rain runoff between the end of Phase III and the beginning of Phase IV. The finding of the complete

sequence of S3 unit (section 1b), in which single horizons show the greater thickness, as well as the lack of structures in all dry horizons (S3-7, S3-11 and S3-13), indicate that currents dropped most of their load without shearing it. Beyond this distance, most flows (from S1-S2 and S3) expanded freely for *ca.* 3 km, over a 2–2.5 km wide plain, where the topography gently declines from 620 to 500 m. In the vicinity of Volcán Chichonal village (3.6–4.7 km E from the crater) the flows were fully turbulent.

The lateral facies variations observed in S2 and S3 deposits between 3 and 3.7 km (sections 3, 4, 107 and 3b, Figure 4a) suggest that the flow behavior was influenced by small obstacles (0.5 – 3 m high) produced by the previous emplacement of PF2. In places where PF2 is lacking (section 107, at 3.6 km), the flows were accelerating as indicated by depositional features such as the low angle cross-stratification of S2-1, the strong erosion of Unit S3 on fallout C, the reduction in thickness and the evidence of traction during transport in all S3 horizons.

Instead, the flows were mostly depositional where PF2 crops out (section 3b at 3.7 km, Figure 5a) because they were laterally blocked. Similarly, S2 and some S1 flows were blocked to the NE by a 120 m topographic obstacle (part of the Caimba anticline; Macías *et al.*, 1997b; García-Palomo

et al., 2004, Figure 2) at distances between 3.5 and 4 km ENE from the crater (sections 103b, 82, 83, 84).

The normal grading observed at the base of S1-3 and S1-7 horizons at 4.8 km (section 67, Figure 4b), indicates that flows had a lower concentration that allowed the segregation of coarser grains at the base of the current (Middleton, 1967); the dilution of flows is supported by the absence of a coarse-grained base in S2-0, S2-1, S2-3 (section 67). Some density currents (S3 unit) were then extremely diluted and vanished in this direction.

In a different way, the first eruptive events produced at the opening of Phase III, and especially S1-1, were extremely energetic and spread radially from the vent reaching up to 7.5 km to the N, 9.5 km to the S, and 10.5 km SE. The pre-eruptive topography had a primary influence to determine the distribution of S1. To the north, the frequent breaks in slope found up to *ca.* 5 km from the vent (sections 76 to 28, Figure 4c) caused changes in the depositional dynamics of S1 within distances of a few hundred meters. As attested by the depositional features of S1-3, a high rate of particle sedimentation (massive to crudely stratified beds; Lowe, 1988) occurred near breaks in slope (sections 53, 51, Figure 4c), while traction conditions (weak plane-parallel beds) occurred in relatively flat areas (sections 52 and 50,

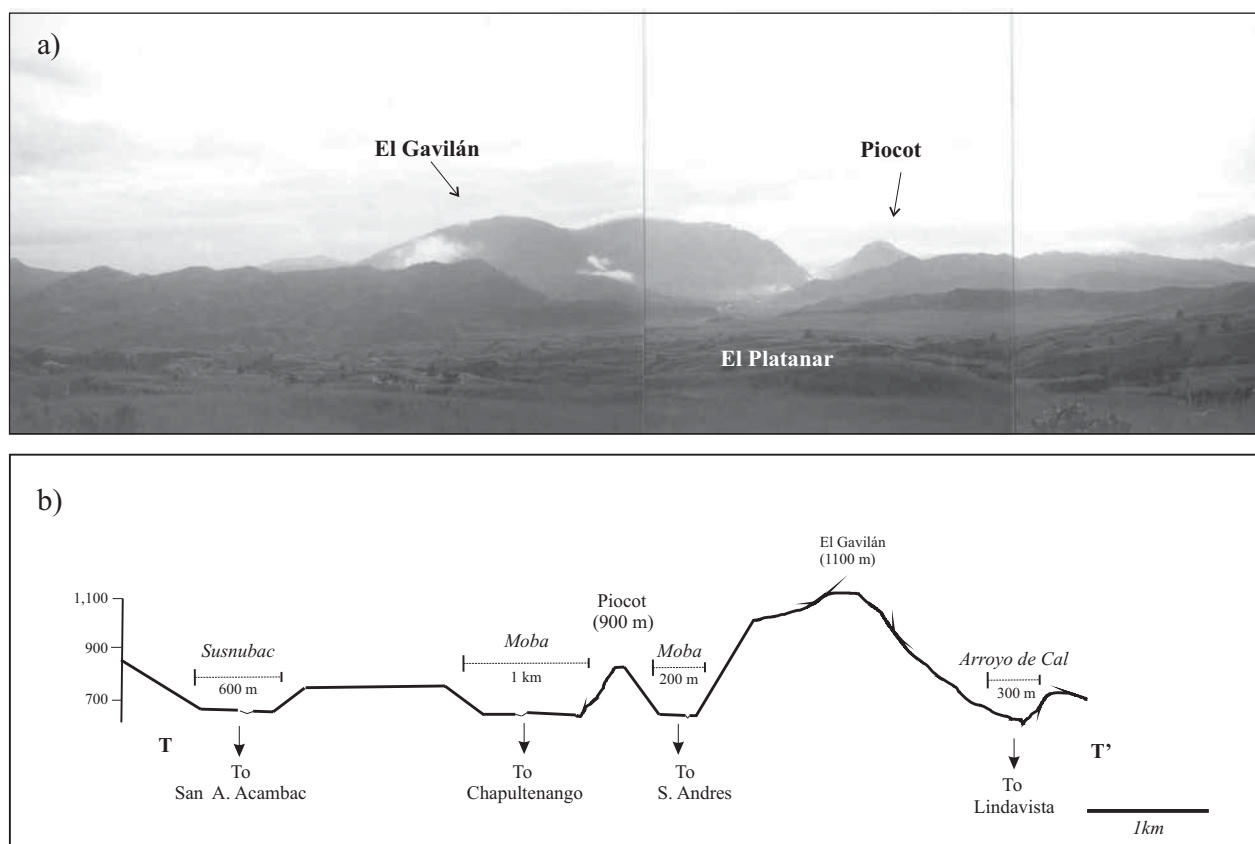


Figure 10. a) Panoramic view from the Somma to the E showing the flat area of El Platanar and Gavilán (1,100 m) and Piocot (900 m) mountains. b) Schematic topographic profile along section TT' (Figure 2) looking toward the crater from the E.

Figure 4c).

To the south, the most energetic flows (S1-0, S1-1, S1-3 and S2-1-3) either followed 500–600 m wide pathways at steep turns of the Magdalena and Susnubac rivers (Figure 2) parallel to the flow direction, or they were blocked by their riverbeds (400 and 300 m in depth) at sites perpendicular to the flow direction. Most currents (S2, S3) were unable to surpass these topographic depressions because of their lower thicknesses, but S1 flows generated during the peak hydromagmatic event. To the E, S1-1 and S1-2 currents were sticky and plastered against steep walls (45° at Cerro El Gavilán, 1,100 m) at distances up to 7.5 km (Figure 4b). Considering the stratified nature of pyroclastic surge clouds (Valentine, 1987) it is reasonable to suppose that S1-1 and S1-2 surge clouds had a similar thickness (1,100 m) at least in this direction.

The dispersal pattern of pyroclastic surge units S1, IU, S2 and S3, is similar to the pattern of fallout deposits A1, B and C (Figure 9). This suggests that near-ground winds, blowing in the same direction of tropospheric winds (<18 km), enhanced the dispersion of the pyroclastic surges (Figure 10 a-b) at greater distances to the NE (up to 9.5 km) and SE (10.5 km). For this reason at the distal tip of S1-1 horizon, the currents had a very weak lateral component. The median diameter and sorting statistical parameters for distal samples of S1-1 and S3-3, and the nature of ash aggregates found in distal sites (Scolamacchia *et al.*, in press) underscore this conclusion.

These observations offer some indications for future hazards related to the emplacement of diluted density currents at El Chichón and similar volcanoes. If we consider the maximum hydromagmatic events as those produced by S1, it is reasonable to conclude that diluted pyroclastic density currents will move in a radius of at least 5 km from the vent with a high kinetic energy, that increase in flat areas or topographic lows. The occurrence of erosive processes contributes to underestimate the magnitude of these events.

CONCLUSIONS

The detailed stratigraphic analysis of pyroclastic surge deposits produced during the 1982 eruption of El Chichón volcano indicates that hydromagmatic activity played an important role during the last phases of the eruption on April 4, 1982. The most violent events occurred at the beginning of phase III (S1) and during the first stages of phase IV (S3). The wide distribution of resulting diluted density currents indicates that they represented the most destructive phenomena because they were poorly confined and had a high horizontal velocity component in proximal and medial areas around the volcano. Although the topography played an important role in controlling the distribution of diluted density currents, strong winds were also important as evidenced by the similar distribution patterns of fallouts

and pyroclastic surge deposits. Therefore wind direction should be taken into account when evaluating the hazards associated with the emplacement of diluted pyroclastic density currents.

ACKNOWLEDGMENTS

The first author is indebted to Felix Sánchez S. and Edilberto Gómez E. for their invaluable help in the field. Municipal authorities and people of Chapultenango, Chiapas, are thanked for providing a roof and assistance during fieldwork. This manuscript greatly benefited from discussions with S. Hughes, and revisions by C. Siebe and A. Di Muro. This work was supported by CONACYT grants (27993-T and 38586-T to JLM), and a CONACYT-CNR bilateral project to JLM.

REFERENCES

- Belousov, A., 1996, Deposits of the 30 March 1956 directed blast at Bezymianni volcano, Kamchatka, Russia, 1996: *Bulletin of Volcanology*, 57, 649-662.
- Brayshaw, A.C., 1984, Characteristics and origin of cluster bedforms in coarse-grained alluvial channels, in Koster, E.H., Steel, R.J., (eds.), *Sedimentology of Gravels and Conglomerates*: Canadian Society of Petroleum Geologist, Memoir, 77-85.
- Büttner, R., Dellino, P., Zimanowski, B., 1999, Identifying magma-water interaction from the surface features of ash particles: *Nature*, 401, 688-690.
- Büttner, R., Dellino, P., La Volpe, L., Lorenz, V., Zimanowski, B., 2002, Thermohydraulic explosions as evidenced by the comparison between pyroclasts and products from molten fuel coolant interaction experiments: *Journal of Geophysical Research*, 107 (B11), 2277 doi:10.1029/2001JB000511.
- Canul, R.F., Rocha, V.L., 1981, Informe geológico de la zona geotérmica de "El Chichonal", Chiapas: Mexico, Comisión Federal de Electricidad, internal report, 38 p.
- Capaul, W.A., 1987, Volcanoes of the Chiapas Volcanic Belt, Mexico: Houghton, MI, Michigan Technological University, M. Sc. thesis, 93 p.
- Carey, S., Sigurdsson, H., 1986, The 1982 eruptions of El Chichón volcano, Mexico; (2) Observations and numerical modelling of tephra-fall distribution: *Bulletin of Volcanology*, 48, 127-141.
- Cas, R.A., Wright, J.V., 1987, Volcanic successions; *Modern and Ancient*: London, Allen and Unwin, 528 p.
- Casadevall, T.J., de la Cruz-Reyna, S., Rose, W.I., Bagley, S., Finnegan, D.L., Zoller, W.H., 1984, Crater lake and post-eruption hydrothermal activity, El Chichón volcano, Mexico: *Journal of Volcanology and Geothermal Research*, 23, 169-191.
- Cioni, R., Sbrana, A., Vecchi, R., 1992, Morphologic features of juvenile pyroclasts from magmatic and phreatomagmatic deposits of Vesuvius: *Journal of Volcanology and Geothermal Research*, 51, 61-78.
- Cole, P.D., 1991, Migration direction of sandwave structures in pyroclastic surge deposits; implication for depositional processes: *Geology*, 19, 1108-1111.
- Cole, P.D., Scarpati, C., 1993, A facies interpretation of the eruption and emplacement of mechanisms of the upper part of Neapolitan Yellow Tuff, Campi Flegrei, Southern Italy: *Bulletin of Volcanology*, 55, 311-326.
- Cole, P.D., Guest J.E., Duncan, A.M., Pacheco, J.M., 2001, Capelinhos 1957-1958, Faial, Azores; deposits formed by an emergent surtseyan eruption: *Bulletin of Volcanology*, 63, 204-220.

- Cough, S.K., Sohn, Y.K., 1990, Depositional mechanics and sequences of base surges, Songaksan tuff ring, Cheju Island, Korea: *Sedimentology*, 37, 1115-1135.
- Crowe, B.M., Fisher, R.V., 1973, Sedimentary structures in base surge deposits with special reference to cross bedding; Ubehebe Crater, Death Valley, California: *Geological Society of America Bulletin*, 84, 663-682.
- Dellino, P., La Volpe, L., 1995, Fragmentation vs. transportation mechanisms in the pyroclastic sequence of Monte Pilato-Rocche Rosse (Lipari, Italy): *Journal of Volcanology and Geothermal Research*, 64, 211-232.
- Dellino, P., Frazzetta, G., La Volpe, L., 1990, Wet surge deposits at La Fossa di Vulcano; depositional and eruptive mechanisms: *Journal of Volcanology and Geothermal Research*, 43, 215-233.
- Dellino, P., Isaia, R., La Volpe, L., Orsi, G., 2001, Statistical analysis of textural data from complex pyroclastic sequences; implications for fragmentation processes of the Agnano-Monte Spina Tephra (4.1 ka), Phlegrean Fields, southern Italy: *Bulletin of Volcanology*, 63, 443-461.
- Dellino, P., Isaia, R., Veneruso, M., 2004a, Turbulent boundary layer shear flow as an approximation of pyroclastic surge: *Journal of Volcanology and Geothermal Research*, 113, 211-228.
- Dellino, P., Isaia, R., La Volpe, L., Orsi, G., 2004b, Interaction between particles transported by fallout and surge in the deposits of Agnano-Monte Spina eruption (Campi Flegrei, Southern Italy): *Journal of Volcanology and Geothermal Research*, 113, 193-210.
- Druitt, T.H., 1992, Emplacement of the 18 May 1980 lateral blast deposit east-northeast of Mount St. Helens: *Bulletin of Volcanology*, 54, 554-572.
- Duffield, W., Tilling, R., Canul, R.F., 1984, Geology of El Chichón volcano, Chiapas, Mexico: *Journal of Volcanology and Geothermal Research*, 20, 117-132.
- Espíndola, J.M., Macías, J.L., Tilling, R., Sheridan, M.F., 2000, Volcanic history of El Chichón volcano (Chiapas, Mexico) during the Holocene and its impact on human activity: *Bulletin of Volcanology*, 62, 90-104.
- Fisher, R.V., 1979, Models for pyroclastic surges and pyroclastic flows: *Journal of Volcanology and Geothermal Research*, 6, 305-318.
- Fisher, R.V., 1990, Transport and deposition of pyroclastic surge across an area of high relief; the 1980 eruption of Mount St. Helens, Washington: *Bulletin of the Geological Society of America*, 102, 1038-1054.
- Fisher, R.V., 1995, Decoupling of pyroclastic density currents; hazard assessment: *Journal of Volcanology and Geothermal Research*, 66, 257-263.
- Fisher, R.V., Schmincke, H.U., 1984, *Pyroclastic Rocks*: Heidelberg, Springer Verlag, 472 p.
- Fisher, R.V., Waters, A., 1970, Base surge bed forms in maar volcanoes: *American Journal of Science*, 268, 157-180.
- Fisher, R.V., Glicken, H.X., Hoblitt, R.P., 1987, May 18, 1980, Mount St. Helens deposits in South Coldwater Creek, Washington: *Journal of Geophysical Research*, 92(B10), 10267-10283.
- García-Palomo A., Macías, J.L., Espíndola J.M., 2004, Strike-slip faults and K-alkaline volcanism at El Chichón volcano, southeastern Mexico: *Journal of Volcanology and Geothermal Research*, 136, 247-268.
- Heiken, G.H., 1971, Tuff rings; examples from the Fort Rock Christmas Valley basin, South Central Oregon: *Journal of Geophysical Research*, 76, 5615-5626.
- Heiken, G.H., Wohletz, K., 1985, *Volcanic Ash*: Berkeley, University of California Press, 1-246.
- Hughes, S.R., 1995, Transport and deposition of pyroclastic surges: Wales, University of Wales, College of Cardiff, PhD Thesis, 500 p.
- Krueger, A.J., Walter, L.S., Bhartia, P.K., Schnetzler, C.C., Krokotov, N.A., Sprod, I., Bluth, G.J.S., 1995, Volcanic sulfur dioxide measurements from the total ozone mapping spectrometer instruments: *Journal of Geophysical Research*, 100, 14,057-14,076.
- Ingram, R.L., 1954, Terminology for the thickness of stratification and parting units in sedimentary rocks: *Geological Society of America Bulletin*, 65, 937-938.
- Inman, D.L., 1952, Measures for describing the size distribution of sediments: *Journal of Sedimentary Petrology*, 22, 125-145.
- Lajoie, J., Boudon, G., Bourdier, J.L., 1989, Depositional mechanics of the 1902 pyroclastic nuée ardente deposits of Mt. Pelée, Martinique: *Journal of Volcanology and Geothermal Research*, 38, 131-142.
- Laronne, J.B., Carson, M.A., 1976, Interrelationships between bed morphology and bed material transport for a small gravel channel: *Sedimentology*, 23, 67-85.
- Lipmann P.W., Mullineaux, D. (eds.), 1981, The 1980 eruption of Mount St. Helens: U.S. Geological Survey, Professional Paper 1250, 844 p.
- Lorenz, V., 1974, Vesiculated tuffs and associated features: *Sedimentology*, 21, 273-291.
- Lowe, D.R., 1988, Suspended-load fallout rate as an independent variable in the analysis of current structures: *Sedimentology*, 35, p. 765-776.
- Luhr, J.F., Logan, M.A.V., 2002, Sulfur isotope systematics of the 1982 El Chichón trachyandesite; An ion microprobe study: *Geochimica et Cosmochimica Acta*, 66(18), 3303-3316.
- Macías, J.L., 1994, Violent short lived eruptions from small sized volcanoes; El Chichón, Mexico (1982) and Styubel, Russia (1907): Buffalo, NY, State University of New York, University at Buffalo, PhD Thesis, 196 p.
- Macías, J.L., Sheridan, M.F., Espíndola, J.M., 1997a, Reappraisal of the 1982 eruption of El Chichón volcano, Chiapas, Mexico; new data from proximal deposits: *Bulletin of Volcanology*, 58, 459-471.
- Macías, J.L., Espíndola, J.M., Taran, Y., Sheridan, M.F., García, A., 1997b, Explosive volcanic activity during the last 3,500 years at El Chichón volcano, Mexico, in IAVCEI General Assembly, Puerto Vallarta, Mexico, Field Trip Guide, 53 p.
- Middleton, G.V., 1967, Experiments on density and turbidity currents; III. Deposition of sediment: *Canadian Journal of Earth Sciences*, 4, 475-505.
- Moore, J.G., Nakamura, K., Alcaraz, A., 1966, The 1965 eruption of Taal volcano: *Science*, 151, 955-960.
- Ritchie, L.J., Cole, P.D., Sparks, R.S.J., 2002, Sedimentology of deposits from the pyroclastic density current of the 26 of December 1997 at Soufriere Hills Volcano, Montserrat, in Druitt, T.H., Kokelaar, B.P. (eds.), The eruption of Soufriere Hills Volcano, Montserrat, from 1995 to 1999: *Geological Society of London, Memoirs*, 21, 435-456.
- Rye, R.O., Luhr, J.F., Wasserman, M.D., 1984, Sulfur and oxygen isotopes systematics of the 1982 eruption of El Chichón volcano, Chiapas, México: *Journal of Volcanology and Geothermal Research*, 24, 109-123.
- Schmincke, H.U., Fisher, R.V., Waters, A., 1973, Antidune and chute and pool structures in the base surge deposits of Laacher See area, Germany: *Sedimentology*, 20, 553-574.
- Scolamacchia T., Macías J.L., Sheridan, M.F., and Hughes, S.R., in press, Morphology of ash aggregates in wet pyroclastic surges of the 1982 eruption of El Chichón volcano, Mexico: *Bulletin of Volcanology*.
- Scientific Event Alarm Network (SEAN), 1982, Volcanic events; El Chichón volcano: Smithsonian Institution, Global Volcanism Program, Scientific Event Alarm Network, Bulletin, 7, 2-6.
- Sheridan, M.F., Wohletz, K.H., 1983, Hydrovolcanism; basic considerations and reviews: *Journal of Volcanology and Geothermal Research*, 17(1-4), 1-29.
- Sigurdsson, H., Carey, S., Espíndola, J.M., 1984, The 1982 eruption of El Chichón volcano, Mexico; stratigraphy of pyroclastic deposits: *Journal of Volcanology and Geothermal Research*, 23, 11-37.
- Sigurdsson, H., Carey, S., Fisher, R.V., 1987, The 1982 eruptions of El Chichón volcano; (3) Physical properties of pyroclastic surges: *Bulletin of Volcanology*, 49, 467-488.
- Sohn, Y.K., 1996, Hydrovolcanic processes forming basaltic tuff rings and cones on Cheju Island, Korea: *Geological Society of America Bulletin*, 108, 1199-1211.
- Sohn, Y.K., 1997, On traction-carpet sedimentation: *Journal of Sedimentary*

- Research, 67(3), 502-509.
- Sohn, Y.K., Cough, S.K., 1989, Depositional processes of the Suwolbong tuff ring, Cheju Island (Korea): *Sedimentology*, 36, 837-855.
- Sohn, Y.K., Cough, S.K., 1992, The Ilchulbong tuff cone, Cheju Island, South Korea; depositional processes and evolution of an emergent, Surtseyan-type tuff cone: *Sedimentology*, 39, 523-544.
- Sohn, Y.K., Cough, S.K., 1993, The Udo tuff cone, Cheju Island, South Korea; transformation of pyroclastic fall into debris flow and grain flow on a steep volcanic cone slope: *Sedimentology*, 40, 769-786.
- Sparks, R.S.J., Walker, G.P.L., 1973, The ground surge deposit; a third type of pyroclastic rock: *Nature*, 241, 62-64.
- Taddeucci, J., Palladino, D.M., 2002, Particle size-density relationships in pyroclastic deposits; inferences for emplacement processes: *Bulletin of Volcanology*, 64, 273-284.
- Tilling, R., 1989, Volcanic hazards and their mitigation; progress and problems: *Review of Geophysics*, 27, 237-269.
- Toon, O.B., 1982, An overview of the effects of volcanic eruptions on climate: *EOS*, 63, 901.
- Valentine, G.A., 1987, Stratified flow in pyroclastic surges: *Bulletin of Volcanology*, 49, 616-630.
- Valentine, G.A., 1998, Damage to structures by pyroclastic flows and surges, inferred from nuclear weapons effects: *Journal of Volcanology and Geothermal Research*, 87, 117-140.
- Valentine, G.A., Fisher, R.V., 2000, Pyroclastic surges and blasts, *in* Sigurdsson, H. (ed.), *Encyclopedia of Volcanoes*: Academic Press, 571-580.
- Walker, G.P.L., 1971, Grain size distribution of pyroclastic deposits: *Journal of Geology*, 79, 696-714.
- Walker, G.P.L., 1984, Characteristics of dune-bedded pyroclastic surge bedset: *Journal of Volcanology and Geothermal Research*, 20, 281-296.
- White, J.D.L., 1991, Maar-diatreme phreatomagmatism at Hopi Buttes, Navajo Nation (Arizona), USA: *Bulletin of Volcanology*, 53, 239-258.
- Wilson, C.J.N., Houghton, B.F., 2000, Pyroclastic transport and deposition: *in* Sigurdsson, H. (ed.), *Encyclopedia of Volcanoes*: Academic Press, 545-554.
- Wohletz, K.H., 1983, Mechanism of hydrovolcanic pyroclastic formation; grain size, scanning electron microscopy and experimental studies: *Journal of Volcanology and Geothermal Research*, 17, 31-63.
- Wohletz, K.H., Sheridan, M.F., 1983, Hydrovolcanic explosions; II. Evolution of basaltic tuff rings and tuff cones: *American Journal of Science*, 283, 385-413.
- Zimanowski, B., Frohlich, G., Lorenz, V., 1991, Quantitative experiments on phreatomagmatic explosions: *Journal of Volcanology and Geothermal Research*, 48, 341-358.
- Zimanowski, B., Büttner R., Lorenz V., 1997, Premixing of magma and water in MFCI experiments: *Bulletin of Volcanology*, 58, 491-495.

Manuscript received: June 15, 2004

Corrected manuscript received: January 17, 2005

Manuscript accepted: March 20, 2005